Technical Report Documentation Page

1. Report No. FHWA/TX-07/0-5202-1	2. Government Accession No.	3. Recipient's Catalog No.
4. Title and Subtitle Determination of Field Suction Values, Hydraulic Properties, and Shear Strength in High PI Clays		5. Report Date August 2005; Revised March 2007 6. Performing Organization Code
7. Author(s) Jorge G. Zornberg, Jeffrey Kuhn, and Stephen Wright		8. Performing Organization Report No. 0-5202-1
9. Performing Organization Name and Address Center for Transportation Research The University of Texas at Austin 3208 Red River, Suite 200 Austin, TX 78705-2650		10. Work Unit No. (TRAIS) 11. Contract or Grant No. 0-5202
12. Sponsoring Agency Name and Address Texas Department of Transportation Research and Technology Implementation Office P.O. Box 5080 Austin, TX 78763-5080		13. Type of Report and Period Covered Technical Report September 2004–August 2006 14. Sponsoring Agency Code

15. Supplementary Notes
Project performed in cooperation with the Texas Department of Transportation and the Federal Highway Administration.

Project Title: Determination of Field Suction Values in High PI Clays for Various Surface Conditions and Drain Installations

16. Abstract
Moisture infiltration into highway embankments constructed by the Texas Department of Transportation (TxDOT) using high Plasticity Index (PI) clays results in changes in shear strength and in flow pattern that leads to recurrent slope failures. In addition, soil cracking over time increases the rate of moisture infiltration. The overall objective of this research is to determine the suction, hydraulic properties, and shear strength of high PI Texas clays. Specifically, two comprehensive experimental programs involving the characterization of unsaturated properties and the shear strength of a high PI clay (Eagle Ford clay) were conducted. These laboratory results allow characterization of the decrease in shear strength with time induced by successive cycles of wetting and drying. Also, the experimental hydraulic results allow quantification of the changes in unsaturated hydraulic properties due to cracking. Assessment of the influence of critical precipitation events is provided.

17. Key Words	18. Distribution Statement
High PI clays, slope stability, hydraulic conductivity, shear strength	No restrictions. This document is available to the public through the National Technical Information Service, Springfield, Virginia 22161; www.ntis.gov.

19. Security Classif. (of report)	20. Security Classif. (of this page)	21. No. of pages	22. Price
Unclassified	Unclassified	88	

Form DOT F 1700.7 (8-72) Reproduction of completed page authorized

Determination of Field Suction Values, Hydraulic Properties, and Shear Strength in High PI Clays

Jorge G. Zornberg, Ph.D., P.E.
Jeffrey Kuhn, E.I.T.
Stephen G. Wright, Ph.D., P.E.

CTR Technical Report:	0-5202-1
Report Date:	August 2005; Revised March 2007
Research Project:	0-5202
Research Project Title:	Determination of Field Suction Values in High PI Clays for Various Surface Conditions and Drain Installations
Sponsoring Agency:	Texas Department of Transportation
Performing Agency:	Center for Transportation Research at The University of Texas at Austin

Project performed in cooperation with the Texas Department of Transportation and the Federal Highway Administration.

Center for Transportation Research
The University of Texas at Austin
3208 Red River
Austin, TX 78705

www.utexas.edu/research/ctr

Disclaimers

Author's Disclaimer: The contents of this report reflect the views of the authors, who are responsible for the facts and the accuracy of the data presented herein. The contents do not necessarily reflect the official view or policies of the Federal Highway Administration or the Texas Department of Transportation (TxDOT). This report does not constitute a standard, specification, or regulation.

Patent Disclaimer: There was no invention or discovery conceived or first actually reduced to practice in the course of or under this contract, including any art, method, process, machine manufacture, design or composition of matter, or any new useful improvement thereof, or any variety of plant, which is or may be patentable under the patent laws of the United States of America or any foreign country.

Notice: The United States Government and the State of Texas do not endorse products or manufacturers. If trade or manufacturers' names appear herein, it is solely because they are considered essential to the object of this report.

Engineering Disclaimer

NOT INTENDED FOR CONSTRUCTION, BIDDING, OR PERMIT PURPOSES.

Project Engineer: Jorge G. Zornberg
Professional Engineer License: California, No. C 056325
P. E. Designation: Research Supervisor

Acknowledgments

The implementation was sponsored by the Texas Department of Transportation. The Project Director was Marcus Galvan, P.E. His help, guidance, and enthusiasm with the project is gratefully acknowledged. The help of Jennie Aguettant, Brian Freilich, John McCartney, and TxDOT personnel from the Bridge Division is also gratefully acknowledged.

Products

Product 1—Recommended field suction values and the effect of surface treatments and drains.
Product 2—Refined and calibrated model for determination of suction and shear strength of high PI clay embankments.

Table of Contents

List of Figures

List of Tables

Chapter 1. Introduction

The Texas Department of Transportation (TxDOT) has experienced problems with recurrent failures in embankments constructed using highly plastic clays. These failures have required periodic maintenance to ensure proper highway safety, which has been costly for the Department. In response, TxDOT initiated an evaluation of the shear strength of high PI (Plasticity Index) clays under various conditions, as well as back-analyses of embankment failures (Stauffer and Wright 1984; Gourlay and Wright 1984; Green and Wright 1986; Rogers and Wright 1986; Kayyal and Wright 1991). Subsequently, Aubeny and Lytton (2003) developed a model for shear strength change with time, based on a continuous diffusion of moisture into a high PI clay slope that results in a decrease in soil suction at depth. Building on these previous studies, this research project has the objective of determining the effect of the passage of time on the shear strength, hydraulic characteristics, and suction profiles on a high PI clay obtained in central Texas (Eagle Ford clay).

One of the objectives of this study is to obtain a refined and calibrated model for the determination of suction and shear strength in high PI clay embankments. The model of embankment strength with time developed by Aubeny and Lytton (2003) involves an analytical solution obtained using simplified assumptions of moisture flow through soil over time. This framework is then used to calculate the soil suction and corresponding shear strength values. Unsaturated moisture flow is modeled as a time-dependent diffusion process, which is realistic only in limited situations. Aubeny and Lytton (2003) used hypothetical suction boundary conditions for soil embankments, and obtained parameters governing moisture flow for undisturbed soil specimens using simple laboratory tests. To simplify the estimation of soil parameters, correlations were used between conventional geotechnical index parameters for compacted clays and the measured moisture diffusion parameters. Aubeny and Lytton (2003) also presented an approach to quantify the increase in moisture flow due to cracking and estimated that the rate of moisture change increases 10 times when cracks are considered in the model. An important aspect that should be emphasized is the conceptual mechanism adopted by Aubeny and Lytton (2003). Specifically, the model developed by Aubeny and Lytton (2003) postulates that surficial failures in high PI clay slopes occur as a consequence of a continuous, time-dependent loss in shear strength due to a continuous, prolonged loss in suction, which is in turn induced by diffusion of moisture through the embankment.

Based on the results gathered as part of this study and on previous significant research on surficial failure mechanisms, this study concludes that failure is not due to a decrease with time (diffusion) of suction, as postulated by Aubeny and Lytton (2003). Instead, the results of this study indicate that surficial failures in high PI clay slopes occur as a consequence of a continuous, time-dependent loss in shear strength due to a continuous development of surface cracks and to a discrete, season-dependent loss in suction, which is in turn induced by precipitation.

Chapter 2. Organization of this Report

This report summarizes the various research components undertaken as part of project 5-9023, sponsored by the Texas Department of Transportation. Specifically, the scope of this project included two significant experimental components undertaken to evaluate (1) the hydraulic properties of an unsaturated high PI clay and the effect of cracking on these hydraulic properties, and (2) the shear strength properties of a high PI clay and the effect of cracking on these shear strength properties.

Section 3 of this report documents the geotechnical characteristics of Eagle Ford clay, the high PI clay used in the two experimental components of this study.

The hydraulic experimental component of this study is summarized in Section 4 of this report, with details of this experimental study provided in the companion report 5-9023-2 (Kuhn and Zornberg 2006).

The shear strength experimental component of this study is summarized in Section 5 of this report, with details of this experimental component provided in the companion report 5-9023-3 (Wright and Aguettant 2006).

The unsaturated hydraulic properties of the high PI clay were used to numerically simulate the performance of exposed embankments under the weather conditions of Austin and Houston. This study allowed determination of suction profiles with time as well as prediction of the depth of moisture fluctuations. This research component is summarized in Section 6 of this report, with details provided in Appendix A of the companion report 5-9023-2 (Kuhn and Zornberg 2006).

Slope stability analyses were conducted to assess the conditions leading to failure of infinite slopes on high PI clays and to assess the need of positive pore water pressures to explain typical failures in high PI clays. This research component is summarized in Section 7 of this report, with details provided in Appendix B of the companion report 5-9023-2 (Kuhn and Zornberg 2006).

Section 8 of this report outlines the site visits conducted as part of this project to evaluate the stability of TxDOT projects involving high PI clays. Details of these site visits are provided in Appendix E of the companion report 5-9023-2 (Kuhn and Zornberg 2006).

An assessment of surface conditions and drain installations was conducted. Also, a preliminary evaluation of the recurrence of precipitation events that would lead to failure of typical slopes in high PI clays for the weather conditions of Austin and Houston is presented in Section 9 of this report. Details of this evaluation are provided in Appendix D of the companion report 5-9023-2 (Kuhn and Zornberg 2006).

A summary of the findings of this study is provided in Section 10 of this report.

Chapter 3. Characteristics of the High PI Clay Used in this Investigation

The soil selected for testing in this study is high PI clay from a slope that had experienced repeated shallow slope failures. The location and description of the slope, along with the physical properties of the soil, are described in this section.

3.1. Site Description

The slope selected for study is located in the Austin District of the Texas Department of Transportation (TxDOT). The slope lies along South Interstate Highway 35 (S IH-35) in the southwest quadrant of the intersection with Hester's Crossing in Round Rock, Texas (Figure 3.1). The slope was created by a cut through Eagle Ford Shale during the construction of IH-35 and later excavated to its existing limits in 1983 when IH-35 was widened. The slope has a height of approximately 21 ft above IH-35 with respect to the southbound exit ramp leading to Sundance Parkway. The grade of the slope after widening IH-35 was approximately 3:1 (horizontal: vertical).

According to TxDOT employees, the first of three failures occurred in approximately 1992 and was repaired by pushing the failed material back into place. The slope failed a second time in the spring of 1999. This time the remediation consisted of excavating beyond the failed material and replacing the excavated material with granular backfill. The existing slope material at the crest of the slope was tilled, moisture conditioned, and compacted according to the TxDOT ordinary compaction method (Item 132 of Texas Standard Specifications 2004). The slope experienced its third failure in the spring of 2003 and was repaired by excavating the material in the failure zone and replacing it with crushed rock. All slope failures occurred after large precipitation events and were located along the same 200-300 ft length of slope. The depth of the slide was generally between 8 ft and10 ft (Galvan 2007).

TxDOT employees stated that this slope remains wet most of the year. This is supported by the presence of Typha latifolia (i.e., cat o'nine tails), which grows in marshy areas, at the base of the slope just north of the failed slope where the slope is believed to drain.

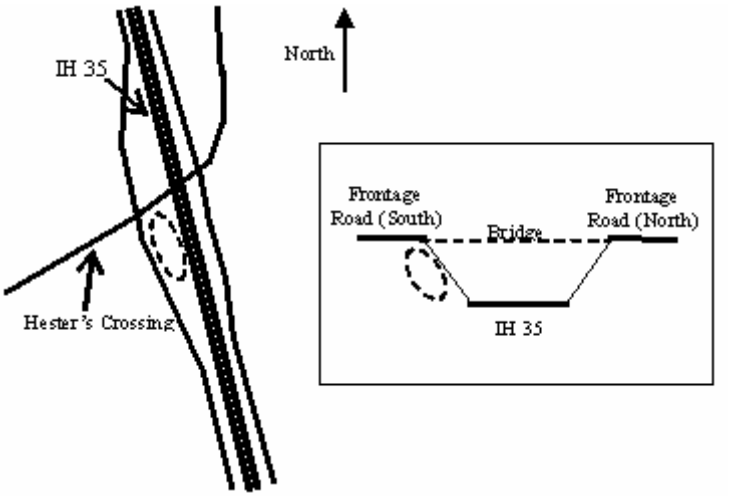

Figure 3.1: Location of failed embankment where testing material was obtained (Borrow area shown as a dashed oval)

3.2. Precipitation Information near the Time of Failures

As previously mentioned, failures occurred following significant rainfall events. Although the exact months in which the failures occurred are not known, it is known that the slope failed in the winter or spring. The total monthly precipitation for the winter and spring of the years when the slope failed (i.e., 1997, 1999, and 2004) are presented in Table 3.1, along with the average monthly precipitation during each year according to reports from the National Oceanic and Atmospheric Administration (NOAA). These precipitation data were gathered at station number 486, COOP ID 417791 Round Rock Texas 3 NE. This is the closest station to the slope. As can be seen in Table 3.1, the monthly precipitations in the winter and spring of the years when the slope failed were higher than the average annual precipitation at least 50% of the time. The average monthly precipitation for the period of time from 1990 to 2005, excluding the years of failure, are also presented in Table 3.1 for comparison.

3.3. Physical Properties of High PI Clay

Geologic maps indicate that the soil in the slope is Eagle Ford Shale, a highly plastic formation of the Cretaceous age. The index properties and compaction curve determined for the Eagle Ford Shale are presented in this section.

Table 3.1: Monthly precipitation in winter and spring of 1992

Month	1992 Total Monthly Precipitation (in.)	Average Monthly Precipitation from 1990-2005 Excluding 1992, 1999, & 2003 (in.)
January	4.34	2.34
February	7.84	2.08
March	4.05	3.04
April	1.12	3.20
May	8.94	4.71
June	3.86	3.96
Average Monthly Precipitation for the Year (in.)	3.68	4.71

3.3.1 Grain Size Distribution

In fall 2004, disturbed soil samples were excavated from a depth of 10 ft with a backhoe and removed from the site for testing. The soil was air-dried, crushed, and processed before testing. The soil removed from the slope was fine-grained and fissile. The color was mostly gray with yellow coloring on some pieces. After being air-dried and processed, the soil appeared tan in color. The soil was dried at a temperature of approximately 120°F, not exceeding 140°F, according to ASTM D 698-00a so that changes in the soil properties would not occur.

The size of the soil particles used to prepare specimens was limited by the equipment used to process the soil. After crushing and grinding the soil, the largest soil particles were smaller than 4.76 mm in diameter. A hydrometer test was conducted according to ASTM D 422-63 on the soil passing the number 10 sieve. Based on a sieve analysis performed on the soil used in the hydrometer test, the initial grain size distribution revealed that only 8.4 % of the soil was finer than 0.075 mm (number 200 sieve); however, the hydrometer test revealed nearly 89.5% of the Eagle Ford Shale was finer than the number 200 sieve. The results of the hydrometer test are shown in Figure 3.2.

3.3.2 Atterberg Limits

Atterberg limits were performed on the processed Eagle Ford Shale according to the procedures outlined in ASTM D 4318. The Atterberg limits for Eagle Ford Shale as well as those for Paris and Beaumont clay, reported by Kayyal and Wright (1991), are presented in Table 3.2. All three soils are high PI clays (CH).

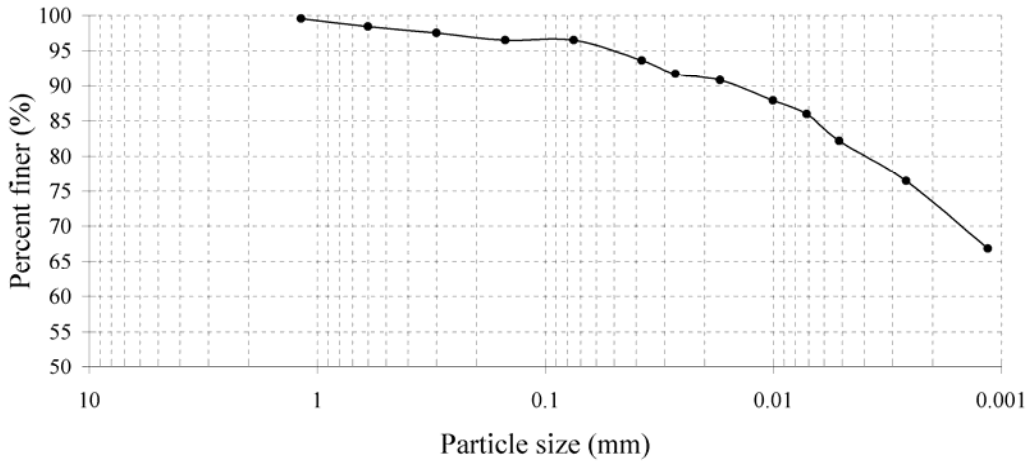

Figure 3.2: Hydrometer analysis for Eagle Ford Shale.

Table 3.2: Index properties of Eagle Ford Shale, Paris Clay, and Beaumont Clay.

Index Property	**Eagle Ford Shale**	**Paris Clay**	**Beaumont Clay**
Liquid Limit (LL)	88%	80%	73%
Plastic Limit (PL)	39%	22%	21%
Plasticity Index (PI)	49%	58%	52%
Clay Fraction (CF)	64%	58%	47.3%
Activity	0.77	1.0	1.1
Unified Soil Classification Symbol (ASTM D 2487)	CH	CH	CH

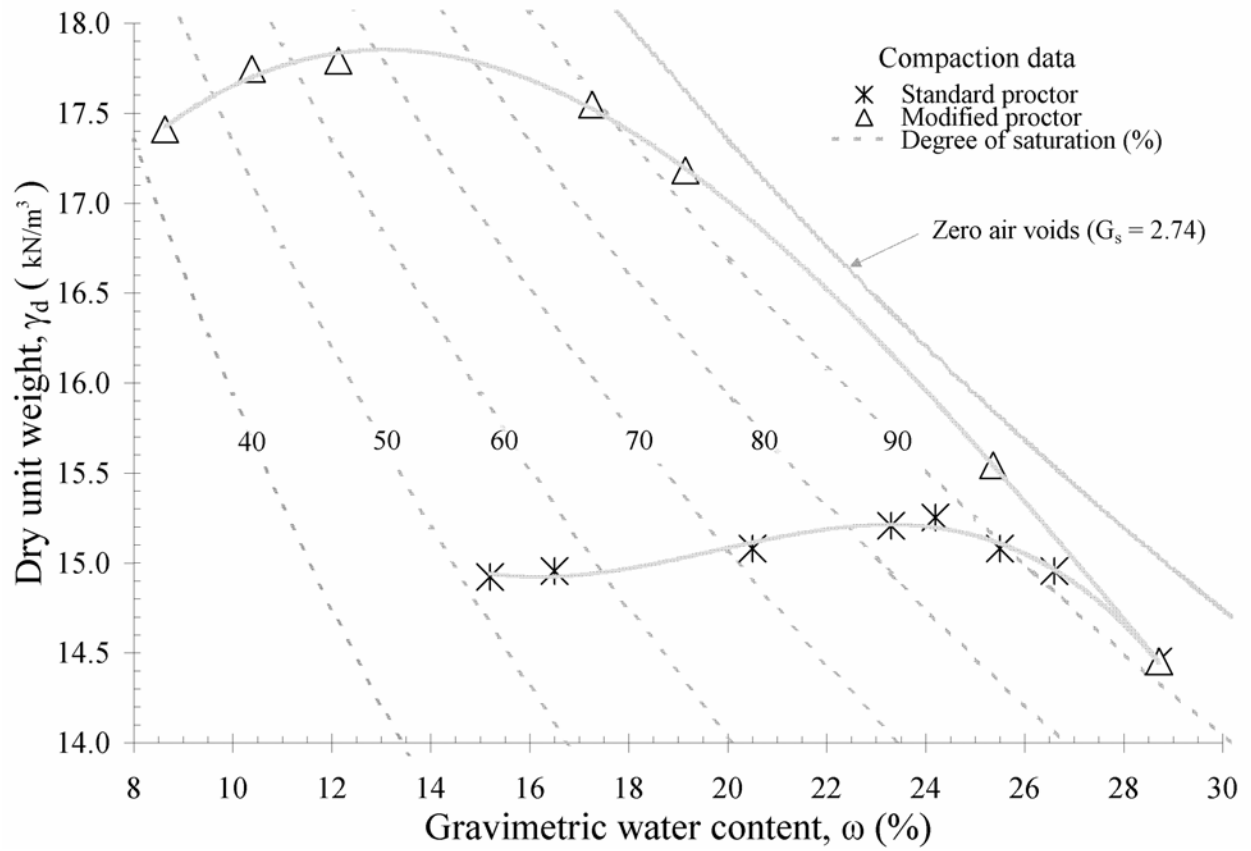

Figure 3.3: Standard and Modified Proctor compaction curves for Eagle Ford Shale.

3.3.3 Compaction Curves

Standard and Modified Proctor compaction tests were performed in accordance with ASTM D 698-00a and ASTM D 1557-02, respectively, to determine the compaction moisture-dry unit weight relationships for Eagle Ford Shale (Figure 3.3). The Standard Proctor optimum moisture content is approximately 24 % with a corresponding maximum dry unit weight of 97 pcf (15.2 kN/m^3). The Modified Proctor optimum moisture content is approximately 14% at a corresponding maximum dry unit weight of 113.5 pcf (17.8 kN/m^3).

3.3.4 Specific Gravity

Two specific gravity measurements were performed on the fraction of soil passing the No. 4 sieve in accordance with ASTM D 854-02. The specific gravity values from the two measurements were approximately 2.731 and 2.742 for an average of approximately 2.74.

3.3.5 Hydraulic Conductivity

A flexible-walled permeameter test was conducted on a compacted specimen of soil with a height-to-diameter ratio of approximately 0.5. The specimen was compacted at a moisture content of approximately 23.6%, which is within 1% of optimum (24%), and a dry unit weight of 98.7 pcf ($\gamma_{d,max}$ = 97.5 pcf). This is comparable to the compaction conditions of the compacted triaxial specimens described in Section 5. After saturation and consolidation at an effective stress

of 4 psi, a hydraulic gradient of 20 was applied between the top and bottom of the specimen. Shallow slope failures typically occur under low effective stresses; therefore, a low effective consolidation stress was used to determine the hydraulic conductivity. The flow rate into and out of the specimen was measured until the ratio of the outflow to inflow was at least 0.99. The hydraulic conductivity was found to be approximately 8×10^{-9} ft/min (4×10^{-9} cm/s).

The hydraulic conductivity was also computed from the consolidation data for a triaxial specimen compacted at a moisture content of 22.5% and a dry unit weight of 96.8 pcf. The specimen had a final effective consolidation pressure of 2 psi. The hydraulic conductivity of this specimen was approximately 1×10^{-8} ft/min (5×10^{-9} cm/s), which is consistent with the value obtained by the flexible-walled permeameter test.

Chapter 4. Experimental Study on the Suction and Unsaturated Hydraulic Characteristics of High PI Clay Embankments

4.1. Overview

An experimental study was conducted as part of this project in order to evaluate the unsaturated hydraulic characteristics of Eagle Ford clay. Determination of the moisture retention properties of this high PI clay, typical of many embankments in central Texas, is necessary for prediction of suction profiles. In addition, the unsaturated hydraulic characteristics of the clay are useful for determination of the depth of moisture fluctuations, which is expected to define the zone over which the shear strength of the clay will be highly affected by the cycles of wetting and drying.

The experimental component of this study regarding hydraulic characterization included a series of evaporation and infiltration experiments conducted to determine the effect of cracking on the hydraulic properties of unsaturated high PI clays. A summary of the main aspects of this study are presented in this section. Details on this experimental component of the research are provided in the companion report 5-9023-2 (Kuhn and Zornberg 2006). The experimental study involved preparation of laboratory specimens and equipment, data collection, data analysis, and an evaluation of the significance of experimental results on the stability of high PI clay slopes. Changes in water content, suction, and weight in the specimen were monitored during controlled infiltration and evaporation. A total of four soil columns were constructed. The first two soil columns were used to investigate the effect of boundary conditions on cracking. The third and fourth soil columns were constructed with lateral restraints.

4.2. Description of the Experimental Hydraulic Program

4.2.1 Scope of the Program

A series of evaporation and infiltration experiments was conducted to characterize the effects of cracking on the hydraulic properties of unsaturated high PI clays. Additionally, experiments were conducted to evaluate the soil placement conditions (i.e., soil conditions immediately after compaction operations). A summary of the experimental testing program is shown in Table 4.1, which shows the main characteristics of the tests conducted to evaluate soil placement conditions and of the soil column tests conducted to characterize the effects of cracking on the hydraulic properties of the high PI clay. The table includes the boundary conditions, soil placement conditions, the sequence of testing, and the variables measured for each experiment.

Table 4.1: Summary of experimental testing program

	Objective	Evaluation of soil placement conditions		Characterization of the effects of cracking on the hydraulic properties of unsaturated highly plastic clay			
	Experiment	Atmospheric boundary condition Controlled Suction	Suction under soil placement conditions HDU measurement	Soil Column 1 Laterally-unrestrained	Soil Column 2 rigid laterally-restrained	Soil Column 3 rigid laterally-restrained	Soil Column 4 rigid laterally-restrained
Boundary Condition	Top	Controlled temp. and humidity 25°C 32, 68, 84, & 97% RH	N/A	Controlled temp. and humidity 25°C 55% RH	Controlled temp. and humidity 25°C 55% RH	Controlled temp. and humidity 23°C 48% RH Constant head 2.5 cm of water	Controlled temp. and humidity 25°C 55% RH
	Sidewall	Unrestrained	N/A	Unrestrained	Restrained Rigid metal screws	Restrained Rigid plastic screws	Restrained Rigid plastic screws
	Bottom	Controlled temp. and humidity 25°C 32, 68, 84, & 97% RH	N/A	No flow	No flow	No flow	No flow
Soil placement conditions		*1* *2* *3*	*1* *2* *3*				
	Gravimetric water content, ω (%)	18 22 25	20 22 24	34	34	22	26
	Volumetric water content, θ (%)	28 34 38	31 34 37	45	45	31	40
	Dry unit weight, γ_d (kN·m^3)	15.0 15.2 15.2	15.1 15.2 15.2	13.0	13.0	15.2	15.1
	Degree of Saturation, S (%)	62 76 64	68 76 83	86	86	76	90
Testing stages	1	Controlled Suction	Equilibration of HDU sensor	Evaporation	Evaporation	Evaporation	Evaporation
	2	N/A	N/A	N/A	N/A	Infiltration	Infiltration
	3	N/A	N/A	N/A	N/A	Evaporation	Evaporation
Variables measured	Soil Water Retention Curve (SWRC)	N/A	N/A	N/A	N/A	Measured (TDR and HDU) 1st Evaporation phase, Infiltration phase, & 2nd Evaporation phase	Measured (TDR and HDU) 1st Evaporation phase Infiltration phase, & 2nd Evaporation phase
	Time-mass relationship	Intact specimen Initial mass and mass at 350 hours	N/A	Intact specimen Intermittent mass via laboratory scale	Cracked specimen Continuous mass via load cell	N/A Instrumentation problems	Measured and reported in Fredlund (2006)
	Hydraulic conductivity function for unsaturated soil (K-function)	N/A	N/A	N/A	N/A	Calculated Unsteady-state profiling method 1st Evaporation phase & 2nd Evaporation phase	Calculated Unsteady-state profiling method 1st Evaporation phase & 2nd Evaporation phase

4.2.2 Boundary Conditions

The evaporation and infiltration experiments involved compacting soil into circular tubes with rigid sidewalls. Specifically, clear polyvinylchloride (PVC) tubing ranging from 152 mm to 203 mm in diameter and 100 mm to 250 mm in length was used. The boundary conditions selected for each experiment included those at the top end of the tube, at the bottom end of the tube, and at the sidewalls of the tube. The temperature and relative humidity were controlled at the top boundary while the tube was closed at its bottom boundary creating a no-flow boundary. In several of the soil columns, screws were used to laterally restrain the soil.

The suction at the boundaries where temperature and relative humidity were controlled was determined using Kelvin's equation (Lu and Likos 2005). Kelvin's equation is typically expressed in terms of total suction, as follows:

$$\Psi_t = -\frac{RT}{\upsilon_{wO}\omega_v}\ln(RH) \qquad \text{Equation 4.1}$$

Where, R = universal gas constant (8.2144 J/mol-K), T = absolute temperature in Kelvin, $\upsilon_{\omega o}$ = saturated vapor pressure of free water in kilopascals at temperature T, and ω_v = molecular weight of water (equal to 18.06 kg/Kmol).

The suction, defined using Kelvin's equation, for relative humidity values ranging from 0 to 100% is shown in Figure 4.1 for temperatures of 0, 20, and 40° C. Over the range of temperatures used during this research component, the effect of temperature on total suction was found to be negligible when compared to that of relative humidity.

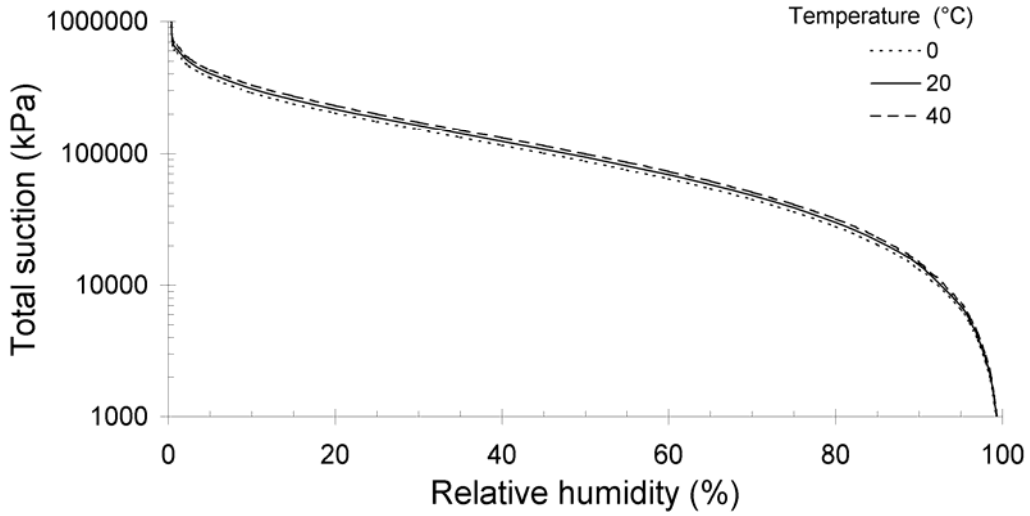

Figure 4.1: Total suction plotted versus relative humidity at various temperatures using Kevin's equation

Evaluation of soil placement conditions also involved compacting soil into circular tubes with rigid sidewalls. Specifically, a 10 mm length of 2 mm thick aluminum tubing with an inner diameter of 54 mm was used for individual soil samples. The temperature and relative humidity were controlled at the top and bottom boundaries. No lateral restraint was used. The suction at the bottom and top boundary conditions was calculated using Kelvin's equation (Equation 3.1),

using the measured temperature and the relative humidity for various saturated salt solutions (Greenspan 1976).

4.2.3 Quantification of Suction under Typical Soil Placement Conditions

Soil conditions after compaction operations define the "initial" suction in the soil. Two series of experiments were conducted to evaluate the effects of soil placement on the initial suction. One series was conducted to evaluate the effect of relative humidity on moisture movement after soil placement, while another series was conducted to measure the initial suction for different soil placement conditions.

To evaluate the effect of relative humidity as a boundary condition, soil samples were compacted using three different placement conditions and were allowed to reach equilibrium under four different values of relative humidity. Different saturated salt solutions were used to maintain relative humidity values of 33%, 68%, 84%, and 97%. The saturated salt solutions used in this experiment and the total suction value corresponding to the relative humidity based on Equation 3.1 for a temperature of 25°C are shown in Table 4.2.

Table 4.2: Total Suction for Various Saturated Salt Solutions

Saturated aqueous salt solution	Relative humidity, RH (%)	Suction, ψ (kPa)
Magnesium chloride	32.8	153,009
Cupric chloride	68.4	52,101
Potassium chloride	84.3	23,365
Potassium sulfate	97.3	3,755

Soil was compacted at gravimetric water contents corresponding to a range from dry to wet of optimum. The soil was compacted into a stack of four 10 mm high and 54 mm inner diameter aluminum rings. The rings were then separated with a wire saw to obtain four specimens of the same initial water content and dry unit weight (Figure 4.2). A soil specimen from each compaction water content group was placed in each of the four relative humidity environments. A 5 mm-thick geonet layer was placed between each soil specimen prior to placement to ensure that the upper and lower boundaries were exposed to the imposed relative humidity. The relative humidity environmental involved an airtight jar containing a saturated salt solution (Figure 4.3). The specimen stacks were placed on a plastic pedestal above the saturated salt solution. After 850 hours, the specimens were removed and placed in an oven to measure their final gravimetric water content.

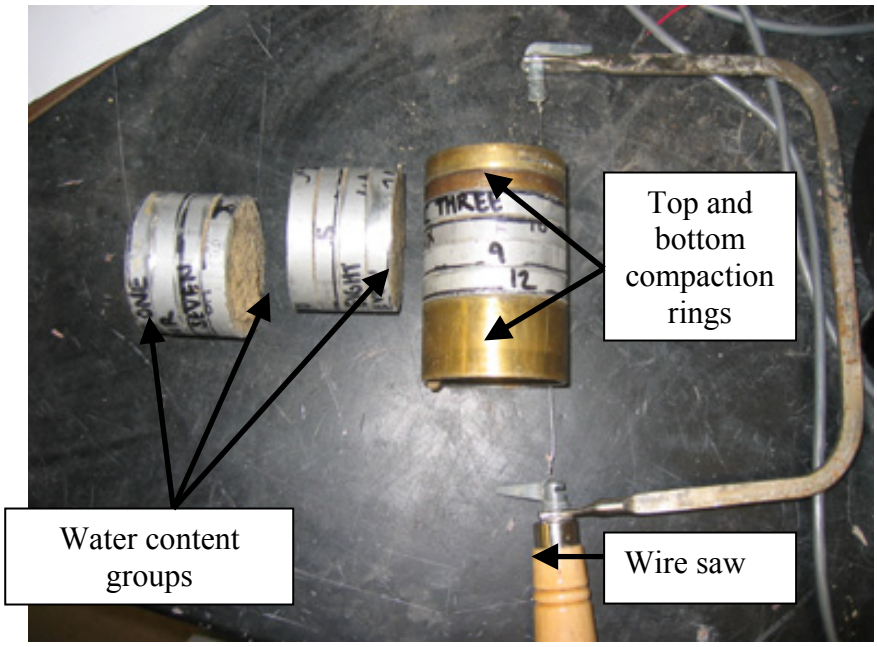

Figure 4.2: Trimming of compaction water content groups for relative humidity experiment

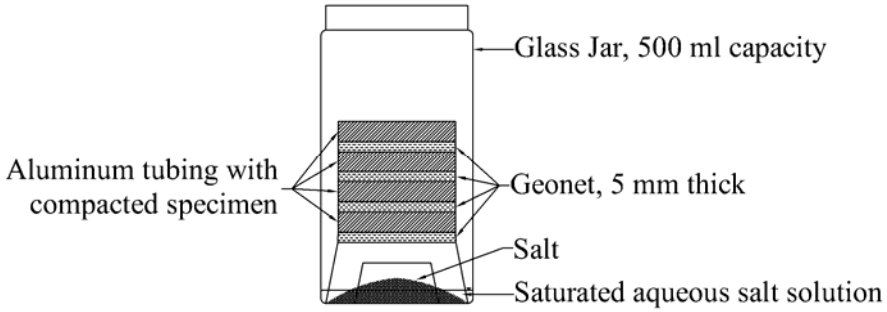

Figure 4.3: Compacted specimens in glass jar containing saturated aqueous salt solution

4.2.4 Soil Columns

A total of four soil columns were constructed to evaluate the cracking pattern and hydraulic properties of high PI clay during cycles of wetting and drying. The main focus of this discussion is on the third and fourth soil columns, which were constructed to measure water content and suction with time while providing lateral restraint against moving. Soil Column 3 is 203 mm in diameter and 250 mm in height. Soil Column 4 was constructed after testing of Soil Column 3 was concluded. Because the upper two sensor layers in Soil Column 4 provided sufficient data for evaluation of the SMRC and K-function of cracked Eagle Ford clay, Soil Column 3 was constructed to a height of 250mm in order to expedite testing. An illustration of Soil Column 3 is shown in Figure 4.4.

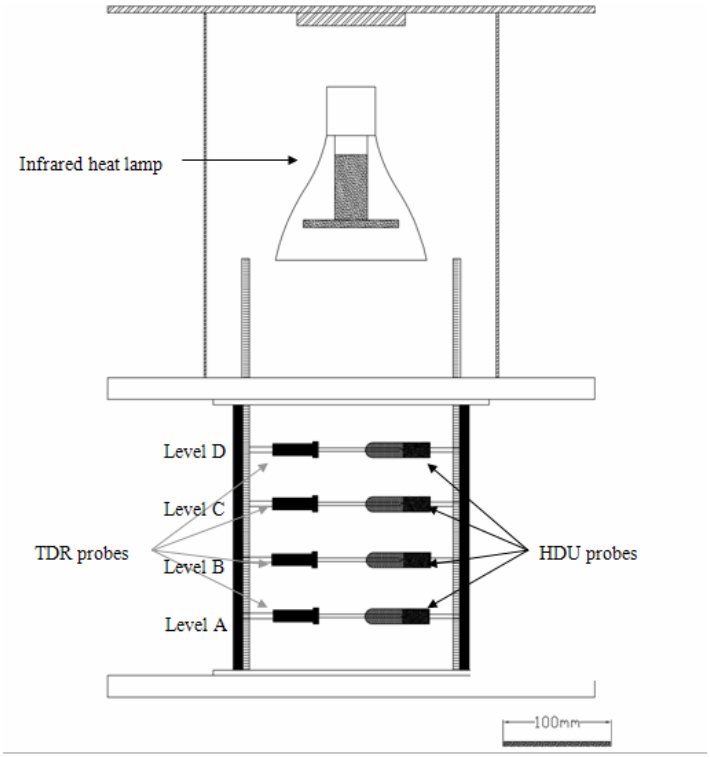

Figure 4.4: Instrumentation setup for Soil Column 3 drying phases

The soil in Soil Column 3 was compacted dry of optimum at (i.e., 22% gravimetric water content) while the soil in Soil Column 4 was compacted wet of optimum (i.e., 26% gravimetric water content). Plastic dry-wall screws were used in Soil Columns 3 and 4. For Soil Column 3, TDR and HDU probes were placed at elevations of 50, 100, 150, and 200 mm, referred to as Levels A, B, C, and D, respectively (Figure 4.4). For Soil Column 4, time domain reflectometry (TDR) and heat dissipation unit (HDU) probes were placed at elevations of 50 and 100 mm. The actual elevation of the probes changed as the soil shrank or swelled. The TDR probes were placed into the soil layers before compaction and HDU probes were placed into the column after compaction. A plan view of the TDR and HDU probes as placed into the soil column is shown in Figure 4.5.

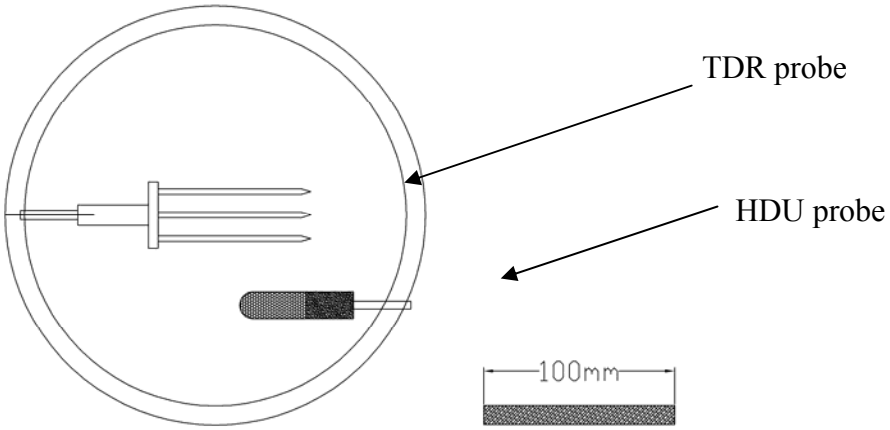

Figure 4.5: Plan view of Soil Column 3 instrumentation

Testing of Soil Columns 3 and 4 included three stages (evaporation, infiltration, and a second evaporation). A schematic representation of the sequences of evaporation (Stages I and II), infiltration (Stages III, IV and V), and a second evaporation (Stages V and VI) in Soil Column 3 is summarized Figure 4.6. The constant head apparatus used during the infiltration stages is shown in Figure 4.7. During the evaporation stages, a fan was used to blow air across the top of the soil specimen and to expedite evaporation (Figure 4.6: Stage I). For Soil Column 3, a constant temperature of 32.2° ± .5° C was maintained using an infrared heat lamp attached to a temperature controller. For Soil Column 4, an infrared heat lamp was not used but ambient temperature was instead measured throughout testing.

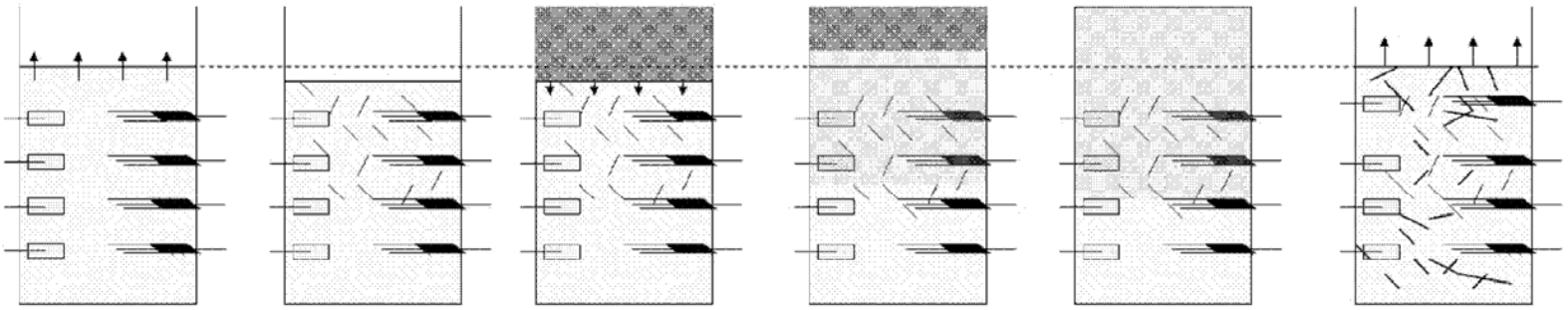

Stages					
I. Start 1st evaporation	II. End 1st evaporation	III. Start infiltration	IV. After 100 hours of infiltration	V. After 1000 hours of infiltration	VI. 2nd evaporation
Summary description					
A 25 cm high specimen was compacted 2% dry of optimum. A fan was then blown across the soil surface to start evaporation.	After 400 hours of evaporation the suction and water content at sensor levels C & D reached steady values constant. Small cracks were visible at the soils surface and the surface had settled 0.1 cm.	A constant head of 2.5 cm was applied at the upper boundary to start infiltration. The soil swelled from 24.9 cm in height to 27.7 cm in height during the first 18 hours of infiltration.	After 100 hours of infiltration an initial wetting front reached the base of the column and a second wetting front reached mid height.	After 260 hours of infiltration, the soil specimen swelled to the top of the infiltration collar at 32.5 cm elevation. Infiltration was continued until 1000 hours when no further downward movement of the second wetting front was observed.	The infiltration apparatus was removed and the soil above 25 cm elevation was removed. A fan was then used to start the 2nd evaporation phase. Significant cracking occurred during the second evaporation stage. After 1050 hours of evaporation testing was stopped.

Figure 4.6: Soil Column 3 timeline

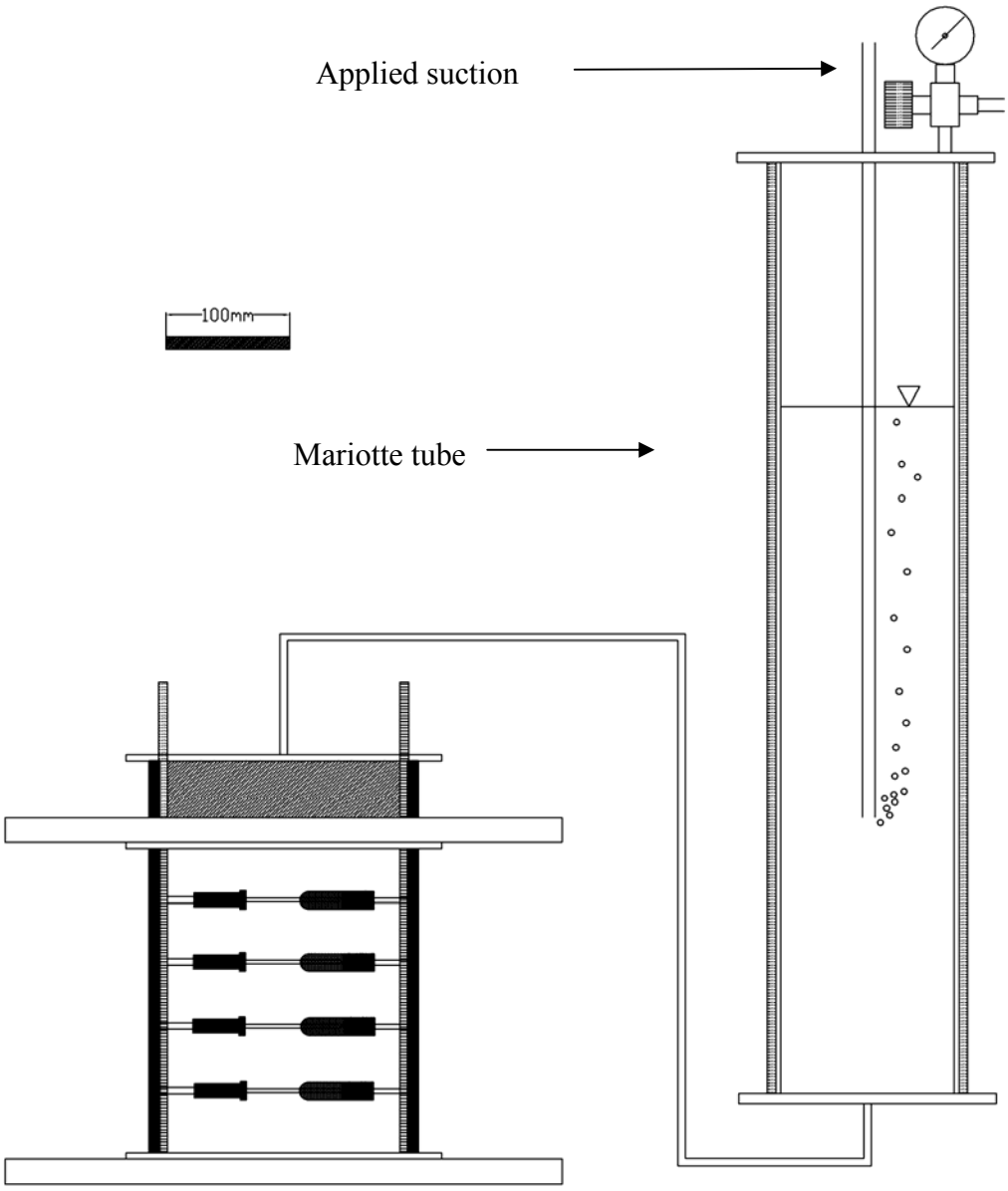

Figure 4.7: Constant head infiltration apparatus for infiltration of Soil Column 3

4.3. Instrumentation of the Soil Columns

TDR probes were used to measure the bulk dielectric constant of a soil. The bulk dielectric constant of the soil is strongly affected by its volumetric water content. The measured bulk dielectric constant of the soil is typically converted to volumetric water content using empirical equations. However, generic relationships have not been found to work well for high PI clays (Roth et al. 1990). Consequently, soil-specific correlations were developed in this study. The soil-specific correlations are compared with Topp's universal equation (Topp et al. 1980) in Figure 4.8.

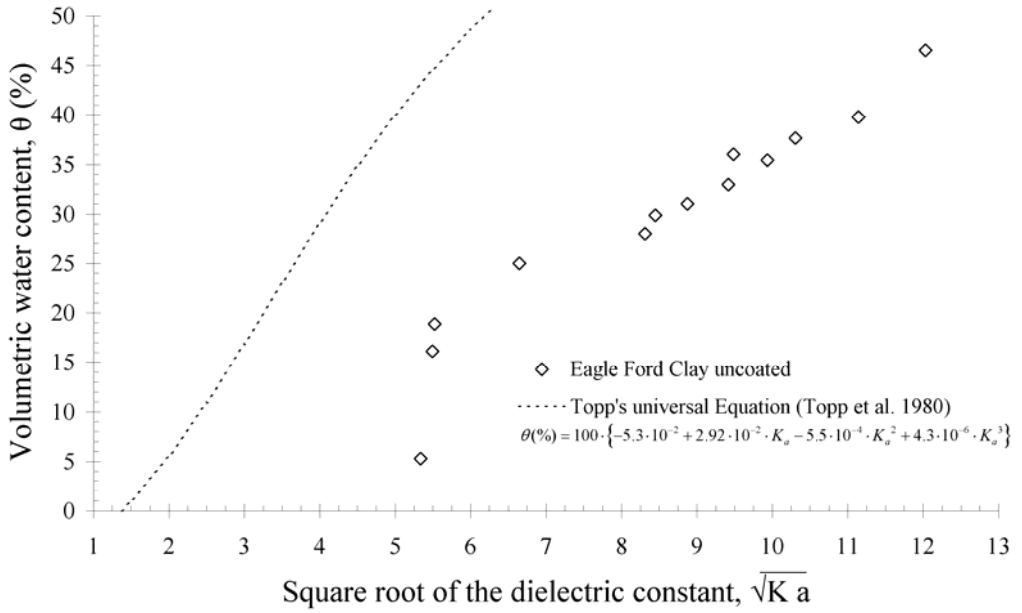

Figure 4.8: The measured and predicted volumetric water content based on measured dielectric constant

The TDR probes and the cable tester used in this research component are manufactured by Soilmoisture Equipment Corporation (Santa Barbara, California). The TDR probes were placed within Eagle Ford clay compacted at gravimetric water contents ranging from 4% to 35 % using standard Proctor compactive effort. Details concerning the calibration procedure are presented in Kuhn (2005) and report 5-9023-2 (Kuhn and Zornberg 2006). The calibration equations obtained in this research component are shown in Figure 4.9. The calibration data is best represented by a bi-linear relationship. A linear relationship between the square root of the measured dielectric constant and the volumetric water content was determined for volumetric water contents up to 19%. A separate linear relationship for uncoated probes was determined for volumetric water contents over 19%.

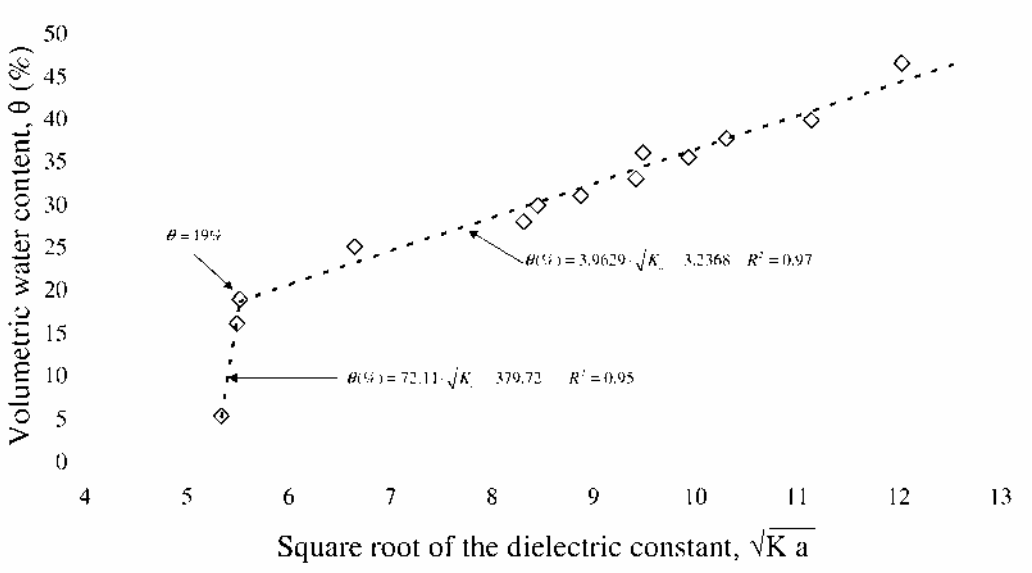

Figure 4.9: Calibrations for coated and uncoated TDR probes in Eagle Ford clay

HDU probes were used to measure the soil suction. A heating element inside the probe is turned on for a period of time and a thermocouple inside of the probe is used to measure the temperature of the probe's porous ceramic body during this time period. The change in temperature that occurs during a selected portion of this time period is defined as the measured temperature rise. The measured temperature rise depends on the thermal properties of the HDU probe and varies with the volumetric water content of the HDU probe and suction of the HDU probe. A calibration relationship consisting of the relationship between temperature rise and suction can be established for individual probes.

The calibration procedure proposed by Flint et al. (2002) was validated in this research component to gain confidence in using non-dimensional temperature rise to calculate suction (Equation 3.2; Equation 3.3). Specifically, the calibration procedure proposed by Flint et al. was validated by saturating HDU probes and using axis translation to impose suction values of 55 and 148 kPa (Figure 4.10). Also, an unsaturated aqueous solution of sodium chloride was used to impose suction values of 300 and 454 kPa. Details concerning these verification procedures can be found in Kuhn (2005).

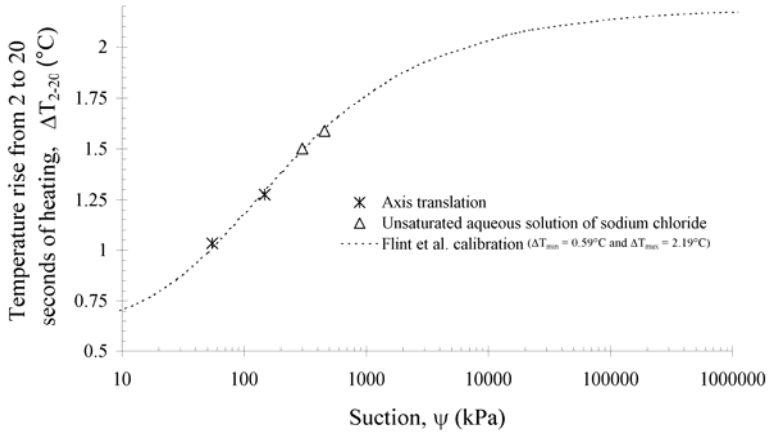

Figure 4.10: Verification of Flint et al.'s calibration procedure

4.4. Summary of Experimental Results

Digital photos of the soil surface, taken during the evaporation stage in Column 1, are shown in Figure 4.11. Geometric cracking patterns were visible on the surface soon after the evaporation stage started. As drying progressed, the intensity of cracking at the surface of the column increased and the soil at the surface of the column became visibly lighter in color. The intensity of cracking continued to increase through the initial 7.3 hours of drying [see Figure 4.11 (a) to (h)]. After 7.3 hours of drying, the specimen separated from the sidewalls of the soil column [see Figure 4.11 (h) to (i)]. Cracks on the surface of the soil specimen partially closed as the soil specimen separated from the sidewalls of the soil column. The separation between the soil specimen and the column sidewall, observed initially at the top of the soil column, propagated down the soil column during the drying process. No significant changes in the surficial cracking pattern took place from 71 hours to 435 hours of drying, when the drying front reached the bottom of the soil column.

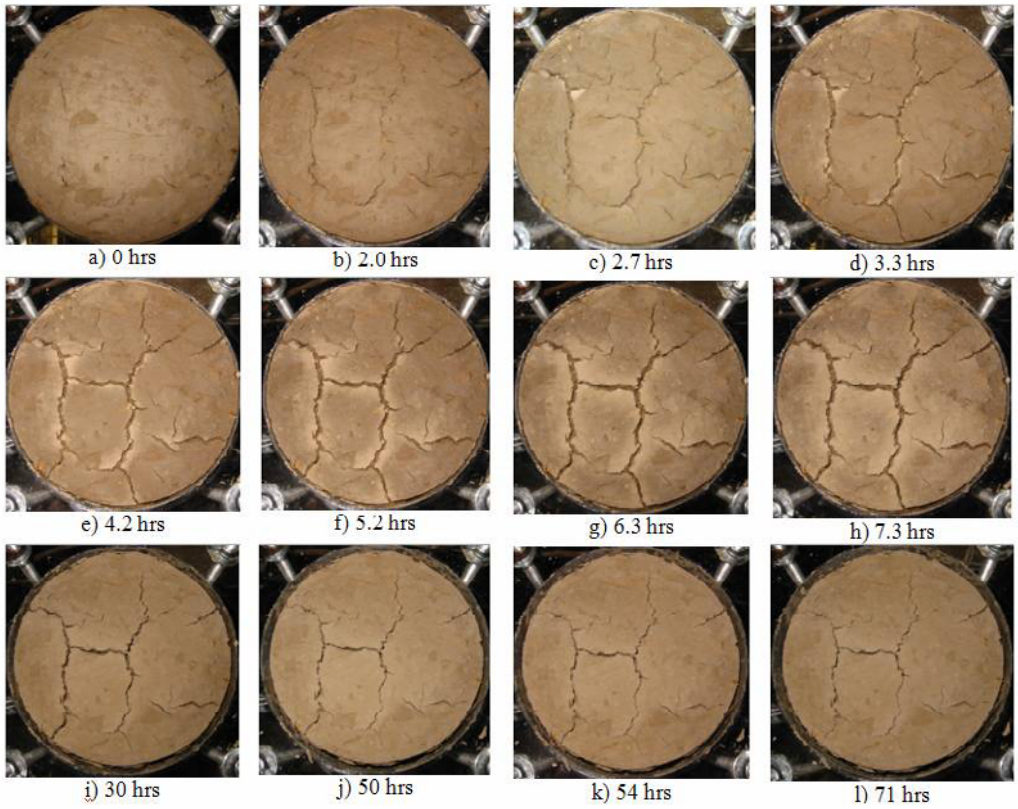

Figure 4.11: Crack formation and closure in Soil Column 1 during drying

Two drying fronts of contrasting water contents were identified based on observation of the color changes in the soil column profile. An image of Soil Column 1 and the two drying fronts, as observed after 48 hours of drying, is shown in Figure 4.12. The first drying (lower front) moving down the soil column was characterized by a darker fringe. The second drying front (upper front) corresponds to the upper boundary of the darker fringe. The reason for these two fronts is speculated to be a reverse capillary break. That is, the upwards flow from the as-placed zone forms a capillary break at the interface with the drier zone. In this case, the hydraulic conductivity of the unsaturated drier zone is less than that of the soil in the darker fringe. This mechanism is expected to lead to water accumulation at the interface between the upper and lower regions. The average thickness of the fringe was 15 mm (ranging from 10 to 20 mm). The average downward velocity of the drying fronts was approximately of 6×10^{-5} cm/s.

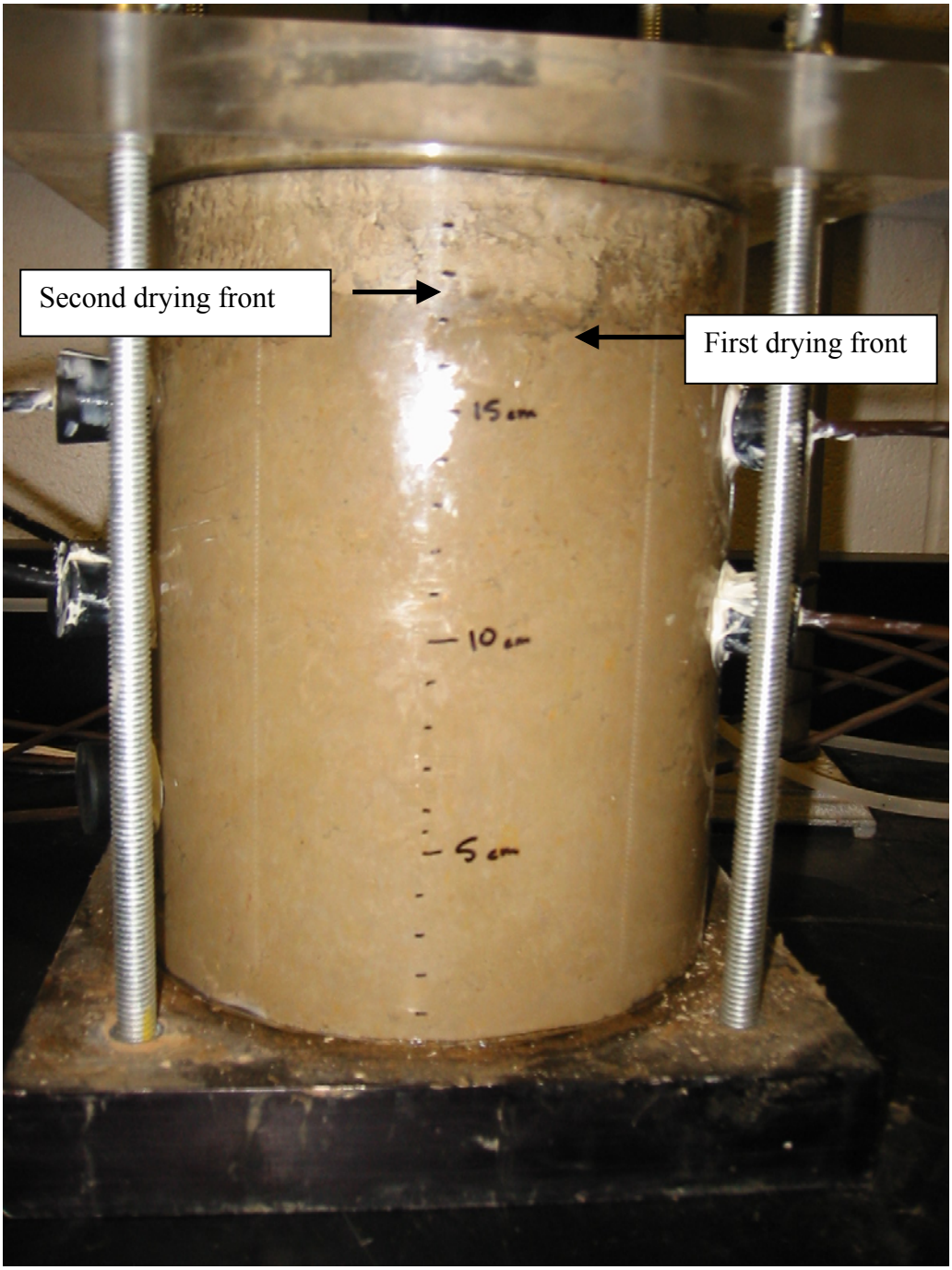

Figure 4.12: Two drying fronts in Soil Column 1 as observed after 48 hours of drying

Data collected from Soil Column 4 is discussed here to illustrate the type of information collected from the columns. The entire dataset is available in Report 5-9023-02 (Kuhn and Zornberg 2006). During the first evaporation stage, the volumetric water content at the upper and lower sensor levels decreased more significantly and at a faster rate for the upper layer than for the lower layer (Figure 4.13). Likewise, the observed suction at the upper layer was greater than the observed suction at the lower layer (Figure 4.14).

The volumetric water content measured during infiltration is shown in Figure 4.15. It is evident that a rapid increase in volumetric moisture content occurred at the upper instrumentation layer. The increase in volumetric moisture content observed at the lower layer was more gradual. Likewise, the suction measured at the upper layer decreased to less than 10 kPa before any measurements of suction could be taken. The suction at the lower level did, however, decrease more slowly and is shown in Figure 4.16. For the lower layer of instrumentation, the suction value at the beginning of testing was taken as the measurement of suction prior to wetting. Because of an instrument malfunctioning, data was not recorded until approximately 130 hours of infiltration. A gradual decrease in suction can be noted between 150 and 300 hours of testing.

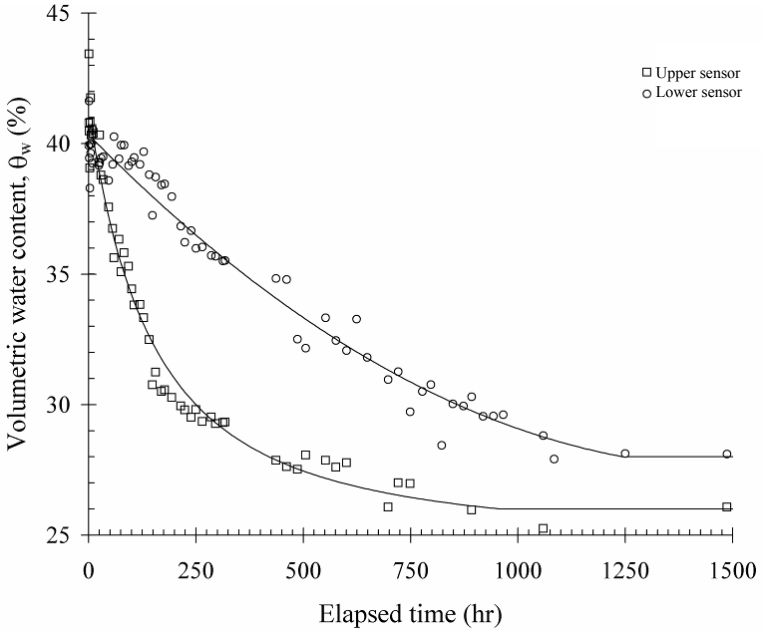

Figure 4.13: Volumetric water content in Soil Column 4 during first evaporation phase, as obtained from TDR measurements

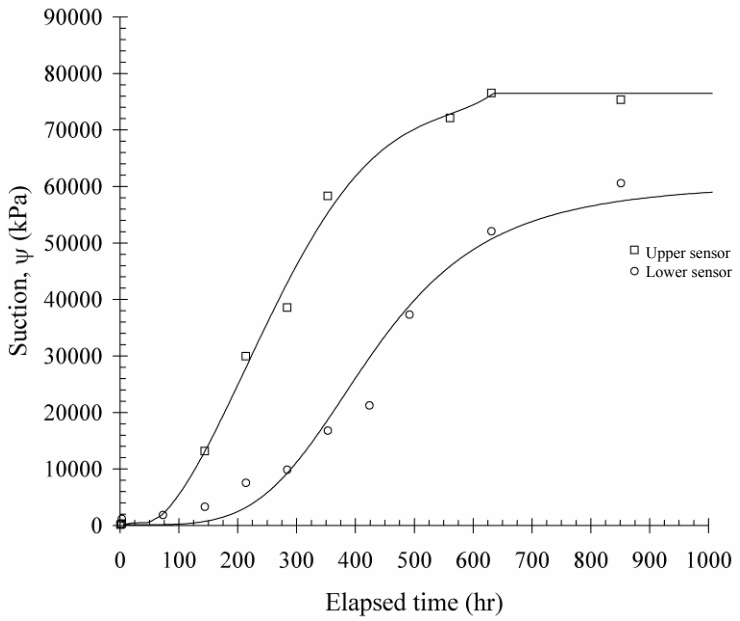

Figure 4.14: Soil suction in Soil Column 4 during first evaporation phase, as obtained from HDU measurements

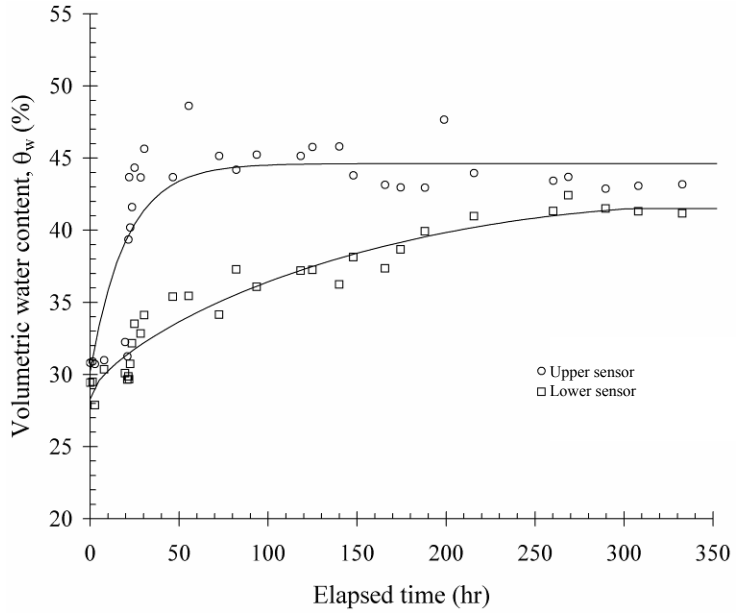

Figure 4.15: Volumetric water content in Soil Column 4 during infiltration phase, as obtained from TDR measurements

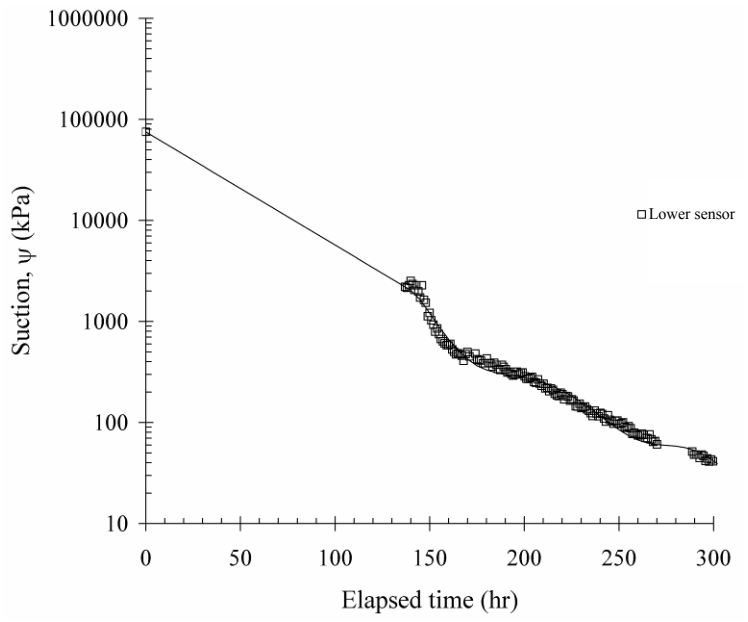

Figure 4.16: Suction in Soil Column 4 during infiltration phase, as obtained from HDU measurements

A second state of evaporation was started when volumetric moisture contents measured at the upper and lower levels had ceased to change significantly with time. The change in volumetric moisture content with time is shown in Figure 4.17. As observed during the wetting phase, a sharp change in volumetric moisture content with time was observed for the upper layer, while a more gradual change in volumetric moisture content with time was observed for the lower layer. The same associated rapid and graduate changes can be observed for the change in suction with time at the upper and lower instrument levels as presented in Figure 4.18. The cracking pattern observed in Soil Column 4 during the second evaporation stage was not significantly different than that observed in Soil column 3.

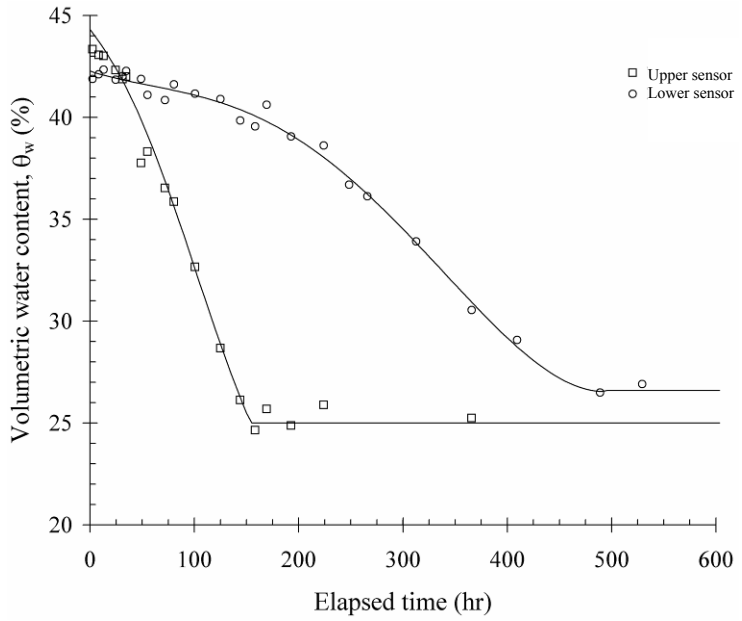

Figure 4.17: Volumetric water content in Soil Column 4 during second evaporation phase, as obtained from TDR measurements

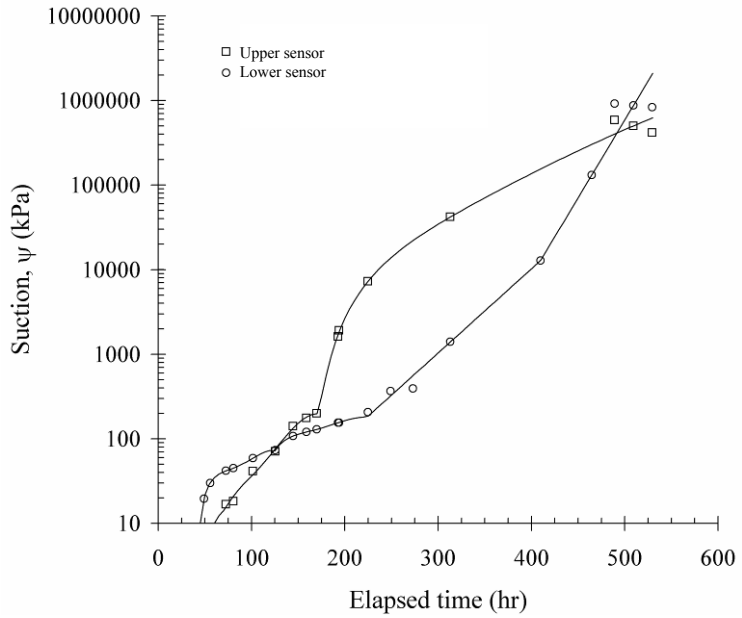

Figure 4.18: Suctions in Soil Column 4 during second evaporation phase, as obtained from HDU measurements

4.5. Analysis of the Data Collected as Part of the Experimental Hydraulic Evaluation

The Soil Water Retention Curves (SMRCs) and Hydraulic Conductivity Functions (K-functions) were determined for Soil Column 3 and 4 using the volumetric water content and suction time histories presented in the previous section. Smooth functions were fit to the time histories for volumetric water content and time to avoid interpreting small fluctuations between subsequent reads as changes in volumetric water content and suction. Another advantage of using these smooth functions is that it allowed for a determination of a continuous SMRC and K-function.

4.6. Effect of Cracking on Water Retention Characteristics

The data collected from Soil Column 3 and Soil Column 4 were used to determine the effects of cracking on the shape of the SMRC. Two SMRC are reported fore each Soil column during each wetting and drying process since suction and volumetric water content were simultaneously monitored at both 5 cm and 10 cm below the surface of the soil. Because highway embankments are typically constructed with soil that is compacted 2% wet of optimum and Soil Column 4 was prepared with soil compacted 2% of optimum, only the results from Soil Column 4 will be presented in this section. The SMRCs calculated for Soil Column 4, prepared with soil compacted 2% dry of optimum, are presented in the companion report 5-9023-2 (Kuhn and Zornberg 2006).

The SMRCs determined for Soil Column 4 are shown in Figure 4.19. From the presented data, it is evident that at a given level of suction, the measured volumetric water content is considerably lower for the second drying phase than for the first. At a particular volumetric water content, this shift would indicate a one to two order magnitude decrease in suction. These results in indicate that the SMRC of the soil varies with depth. Consequently, to model the hydraulic response of the system, it may be necessary to consider a multilayered system with significant contrasts in hydraulic conductivities. The presence of contrasting hydraulic conductivities with depth may have significant implications for the stability of the slope.

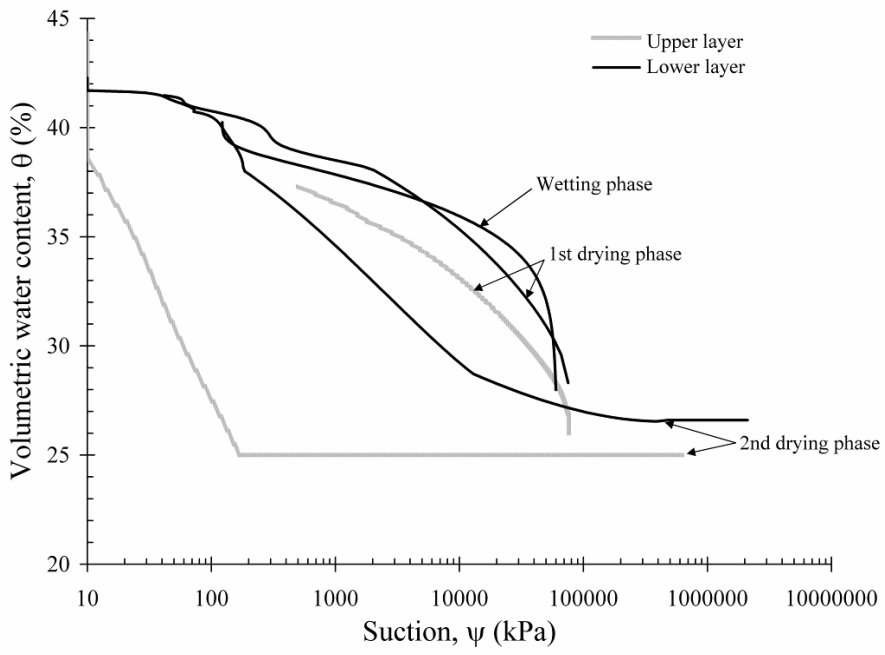

Figure 4.19: Soil water retention curves for Soil Column 4, soil compacted 2% wet of optimum

4.7. Effect of Cracking on the Rates of Evaporation and Infiltration

The effect of cracking on the rates of evaporation and infiltration were determined from the data collected from Soil Columns 1 and 2. Details on the analysis of the data are presented in the companion report 5-9023-3 (Kuhn and Zornberg 2006). Because the soil in Column 1 was allowed to shrink freely during drying and the soil in Column 2 was restrained and cracked during drying, the two can be compared. Based on the change in mass of the soil column with time, the evaporation rate of water can be determined. In order to compare the results, the evaporation rate calculated for Soil Column 2 was divided by the evaporation rate calculated for Soil Column 1. The results are presented in Figure 4.20. From the ratio of the evaporation rates, it is evident that the initial evaporation rate from Soil Column 2 was at least twice that from Soil Column 1. The ratio of evaporation rates between these two columns decreased up until the end of testing but the evaporation rate from Soil Column 2 exceeded that from Soil Column 1 throughout testing.

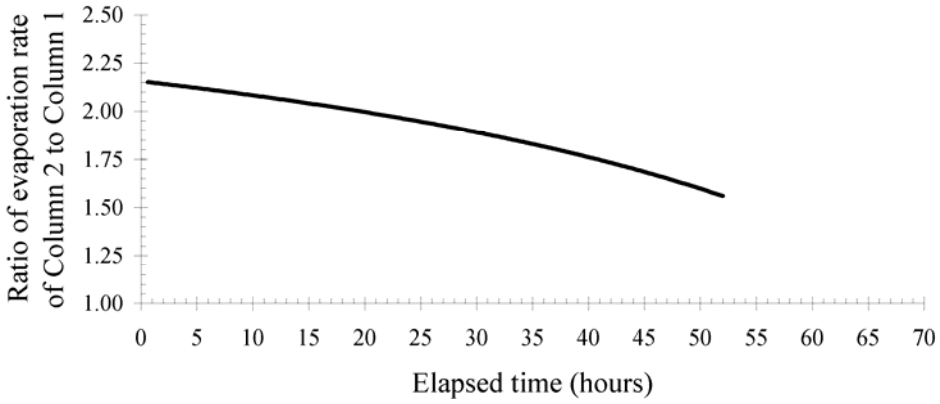

Figure 4.20: Ratio of evaporation rates from Soil Column 1 and Soil Column 2

4.7.2 Determination of the K-function from Soil Column 3 and Soil Column 4 Results

The K-function was determined for both the first and second drying phases using the instant profiling method (Daniel 1983; Wendroth et al. 1993; Meerdink et al. 1996). The instant profiling method involves calculating the K-function of a soil profile during infiltration or evaporation using measured suctions and volumetric water contents. A derivation of the instant profile method is provided in the companion report 5-9023-2 (Kuhn and Zornberg 2006).

4.7.3 Effect of Cracking on the K-function

The hydraulic conductivity functions calculated for Soil Column 4 are shown for the first and second drying phases in Figure 4.21. The K-function measured during the second drying phase indicates higher measured hydraulic conductivities at a given suction level for the second drying phase than for the first drying phase. It can, however, be noted that the hydraulic conductivity function measured during the first and second drying phases have approximately the same slope in log-log space at suctions higher than approximately 200 kPa. This may indicate cracking shifts the position of the k-function but does not significantly change its slope. Accordingly, it appears as though the combined effect of cracking occurring during the first evaporation stage, swelling occurring during the second evaporation stage, and cracking occurring during the second evaporation stage significantly changed the range of hydraulic conductivity at a given suction value.

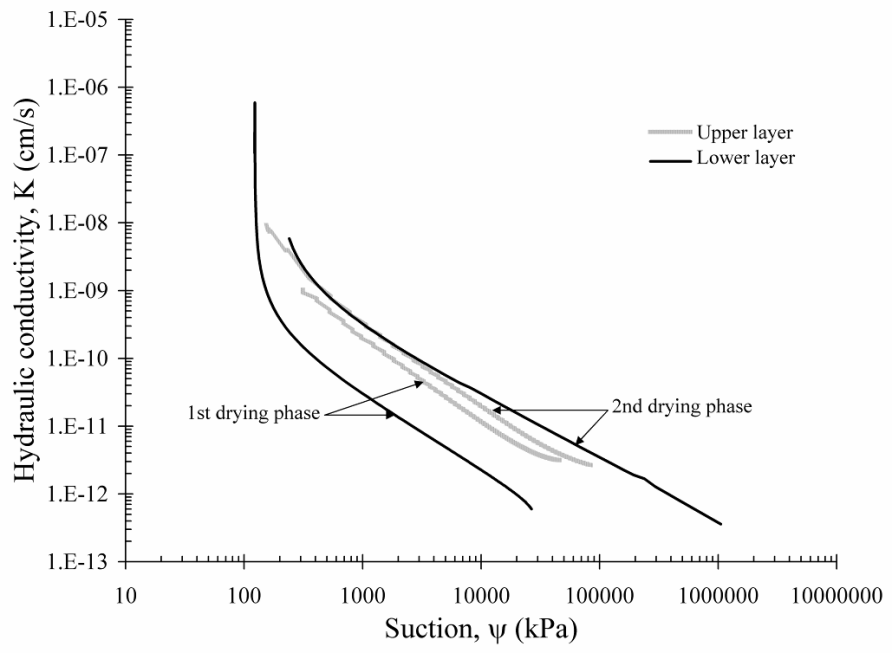

Figure 4.21: Hydraulic conductivity function for Soil Columns 4, compacted 2% wet of optimum

4.8. Summary of Findings

A series of evaporation and infiltration experiments were conducted on compacted Eagle Ford clay to investigate the effect of cracking on the suction profiles and hydraulic properties of unsaturated high PI clays. The following conclusions can be drawn:

- A long-term evaporation process (i.e., an increase in suction rather than a decrease in suction) is expected for typical soil placement conditions and typical weather conditions in Texas. Specifically, evaporation will occur for relative humidity values below 97% in highly plastic soil placed under typical soil compaction. Consequently, because suction within the soil embankment is expected to increase with time as a result of continued exposure to the environment, discrete precipitation events lead to instability due to infiltration.

- Small changes in placement water content produce significant changes in initial suction. For example, the initial suction for Eagle Ford Clay compacted 2.5% dry of optimum is 100,000 kPa while the initial suction is only 100 kPa if the soil is compacted 2.5% wet of optimum.

- The evaporation rate in high PI clays compacted wet of optimum was found to be twice as high in clays after cracks develop than the evaporation rate from intact clay.

- The shape of the soil-water retention curve of high PI clays is significantly affected by the development of cracks. Specifically, the slope of the soil water retention curve was found to increase after cracking.

- The relationship between the hydraulic conductivity and the volumetric water content of unsaturated Eagle Ford clay is significantly affected by cracking. No clear trend between hydraulic conductivity and volumetric water content was found after cracking. The hydraulic conductivity of unsaturated Eagle Ford clay after cracking ranges from 2×10^{-10} cm/s to 3×10^{-7} cm/s for volumetric water content values ranging from 20% to 50%. This suggests that flow is controlled by cracking but apparently independent of the volumetric water content of the soil.

- Soil profiles of high PI clay affected by cracking are expected to have layers of different hydraulic properties. That is, the hydraulic response of exposed slopes of high PI clay may involve a multilayered system with significant contrasts in soil water retention characteristics and hydraulic conductivity values.

Chapter 5. Experimental Study to Define a Refined and Calibrated Model for Determination of the Shear Strength of High PI Clay Embankments

5.1. Overview

Previous research has shown that cyclic wetting and drying can reduce the shear strength of compacted high PI clays to the fully softened shear strength. Fully softened shear strengths are applicable to first-time slides in natural and excavated slopes of stiff fissured over-consolidated material where there has also not been any prior large shear displacement. The fully softened shear strength is also applicable to compacted slopes of high plasticity clays and shales exposed to wetting and drying. The failure envelope for fully softened conditions passes through the origin of a Mohr diagram. It should be noted, however, that although there is no cohesion intercept, the failure envelope is curved at low effective stresses.

Accordingly, a laboratory investigation was conducted to determine the shear strength of Eagle Ford clay that had experienced seasonal wetting and drying in the field. Tests were performed using procedures that were similar to those used by Kayyal and Wright (1991) to test Paris and Beaumont clay. Specimens were prepared by compaction and subsequent cyclic wetting and drying, and by normally consolidation from a slurry. This section presents a summary of the experimental testing program conducted as part of this project. A detailed description of the experimental data and of the analysis of shear strength results is provided in the companion report 5-9023-3 (Wright and Aguettant 2006).

5.2. Testing Procedures

The experimental testing program included (1) a series of tests on as-compacted specimens, (2) a series on specimens normally consolidated from a slurry and (3) a series of specimens prepared by compacting the specimens and then subjecting them to cyclic wetting and drying before testing in the triaxial apparatus. Isotropically consolidated-undrained triaxial compression tests with pore water pressure measurements were performed on the various specimens of Eagle Ford Shale according to the American Society for Testing and Materials' (ASTM) D 4746-02. The purpose of the tests on the specimens normally consolidated from a slurry and those subjected to cyclic wetting and drying was to determine the fully softened shear strength of Eagle Ford Shale. The specimens tested in the as-compacted state served as a basis for comparison and judging the magnitude of softening effects. The stress paths and failure envelopes along with the stress-strain curves are presented and compared in sections 5.3 to 5.5 for each group of specimens. Details on the procedures for preparation of specimens subjected to cycles of wetting and drying (test series 3) are descried in this section. Details on the procedures for preparation of specimens for the other two series are provided in the companion report 5-9023-3 (Wright and Aguettant 2006).

The specimens subjected to cyclic wetting and drying were prepared from the fraction of soil passing a number 40 sieve and compacted to a moisture content of approximately 23%, which is within 1% of the optimum moisture content (24%). After mixing with water, the soil was allowed to equilibrate for at least 16 hours in a humidity room prior to compaction. The

specimens were compacted in eight lifts with 45 blows per lift. After each specimen was compacted, the top of the specimen was trimmed flush with the top of the mold, the mold was disassembled, and the specimen was weighed. The trimmings were used to obtain an initial moisture content for the specimen in the compacted state. For wetting and drying, the compacted specimens were placed in special specimen holders designed by Kayyal and Wright (1991). The specimen holders consist of a cylindrical metallic screen approximately 1.7 inches in diameter, resting on a screen base supported by acrylic rings and threaded rods. The square openings in the screen are 0.425 mm in size. The screen allows water to infiltrate the specimen from all sides while preventing the specimen from disintegrating completely. The apparatus used to hold the specimen during the wetting and drying process is pictured with a compacted specimen in Figure 5.1. The specimens were subjected to twenty cycles of wetting and drying. Kayyal and Wright (1991) determined that each cycle should consist of a period of drying and wetting with the first *cycle* entailing wetting, drying, and rewetting. Each wetting and drying period lasted 24 hours, after which Kayyal and Wright (1991) observed no significant change in moisture content. Kayyal and Wright also found that after twenty cycles, there was no apparent further particle breakdown.

During the wetting phase, each specimen was submerged in an individual 2,000-milliliter beaker filled with distilled water (Figure 5.2). Care was taken to ensure that the specimens were submerged at all times. Water was added as necessary. During the drying phase, the specimens were placed in a constant temperature and constant humidity room set at a temperature of 60°C (140°F) with an average relative humidity of 5 %.

Following the last wetting stage, the specimen and its holder were removed from the water, and excess free water was allowed to drain from the specimen before trimming occurred (approximately 5 minutes). The top acrylic ring was removed from the specimen holder and a cylindrical stainless steel cutting tube with a sharpened bottom edge was pushed vertically down on the specimen. The cutting tube has a length of 5 in. with an inner diameter of 1.5 inches. When the cutting tube reached the underlying screen bottom of the specimen holder, the cylindrical screen and middle acrylic rings were removed. Soil was scraped off the cutting tube and used to obtain an estimate of the initial moisture content. A circular piece of filter paper was placed on the bottom of the specimen. A specially designed acrylic extruder, as described in Aguettant (2005) and report 5-9023-3 (Wright and Aguettant 2006), was then used to remove the specimen from the cutting tube.

Figure 5.1: Cyclic wetting and drying specimen holder and compacted specimen

Figure 5.2: Submerged specimens during the wetting portion of cyclic wetting and drying test series

5.3. As-Compacted Consolidated-Undrained Triaxial Compression Specimens

Five consolidated-undrained triaxial compression tests with pore water pressure measurements were performed on as-compacted specimens using a range of effective consolidation pressures from 2 psi to 40 psi.

The stress-strain curves for the as-compacted specimens are presented in Figure 5.3. It appears that the higher the effective consolidation pressure, the more softening occurs once the peak strength is reached. Specimens reached failure corresponding to points where the stress path became approximately tangent to the failure envelope at axial strains ranging from 1% to 7%. The test of the as-compacted specimen with an effective consolidation pressure of 15 psi was ended inadvertently at a much lower strain than it should have been; however, from Figure 5.4 it appears that the specimen had reached failure according to the point of stress path tangency to the failure envelope.

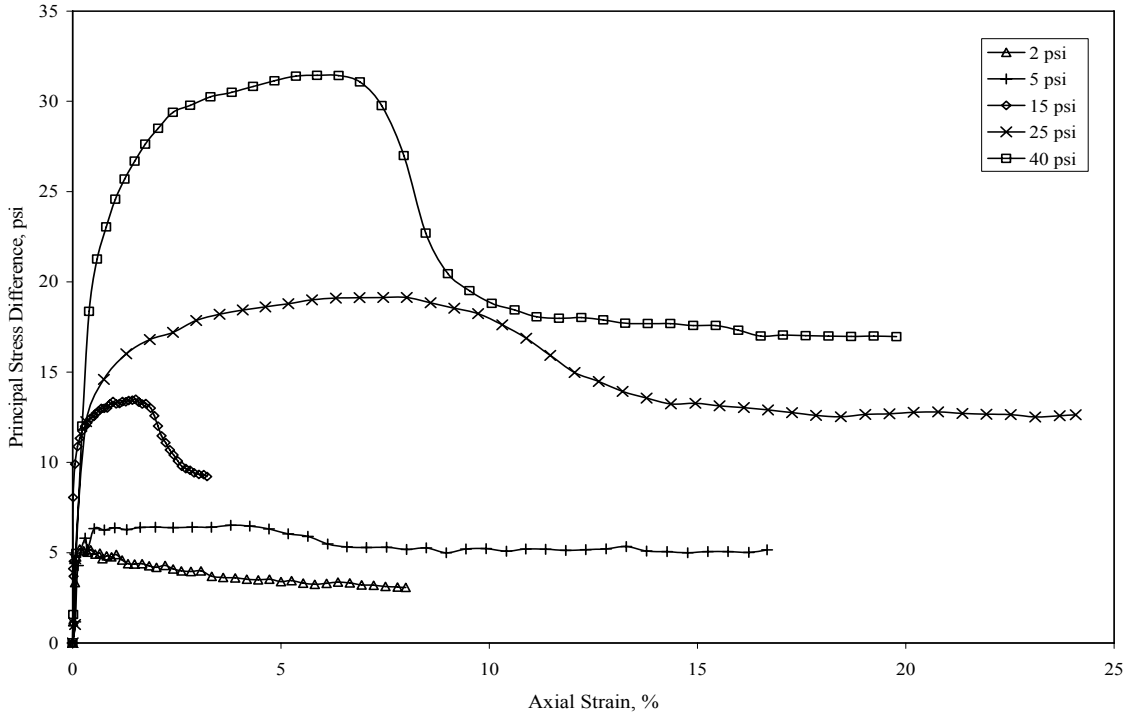

Figure 5.3: Stress-strain curves for as-compacted specimens of Eagle Ford Shale

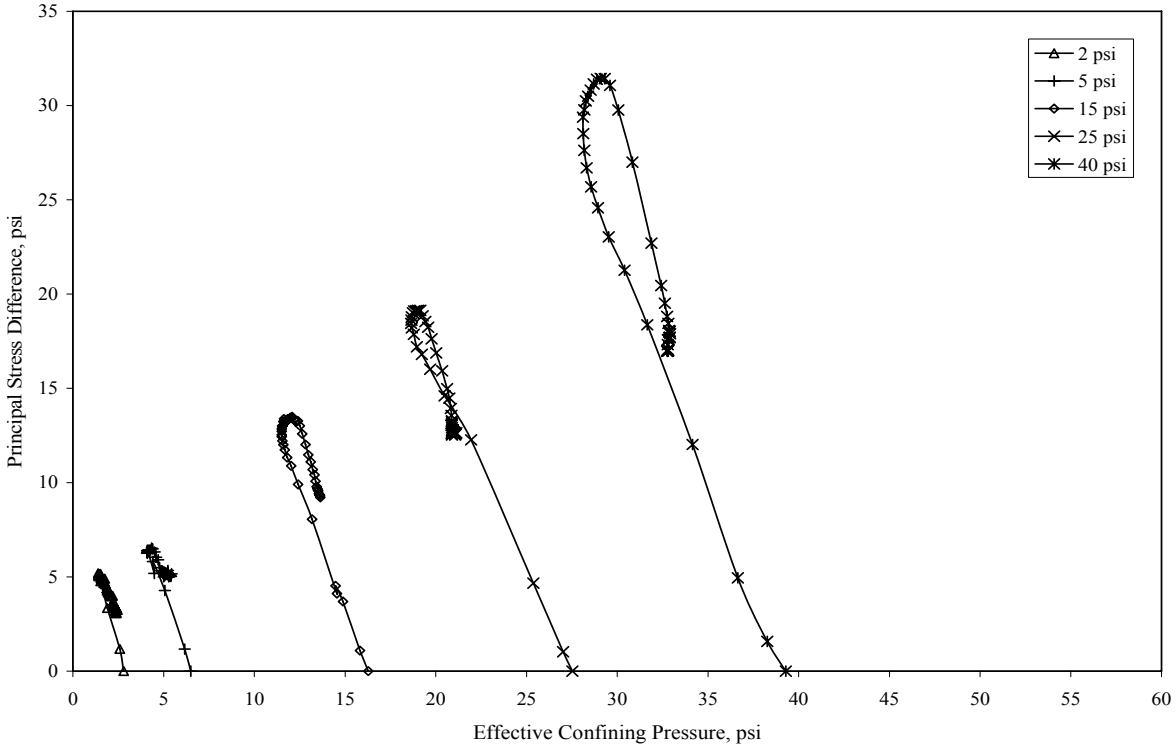

Figure 5.4: Modified Mohr-Coulomb diagram for as-compacted specimens of Eagle Ford Shale.

The effective stress paths for the specimens tested in the as-compacted state are shown in Figure 5.2. The effective stress paths in Figure 5.2 first tend to the left until the peak principal stress difference is reached and then curve to the right. This behavior is common of slightly over-consolidated soils. The modified Mohr failure envelope, based on points where the stress path is approximately tangent to the failure envelope, is presented in Figure 5.5. The failure envelope shows little if any curvature. The shear strength parameters based on a linear failure envelope are $c' = 1.5$ psi and $\varphi' = 16.5°$ for the as-compacted conditions. Bailey and Stroman (1992) reported values of the effective cohesion for undisturbed specimens of Eagle Ford Shale that were obtained from compacted fills ranging from 0.1 to 0.2 tsf (1.39 to 2.78 psi) and values of the effective friction angle ranging from 17 to 22 degrees. Thus, the as-compacted strength agrees well with previously documented strengths of Eagle Ford Shale.

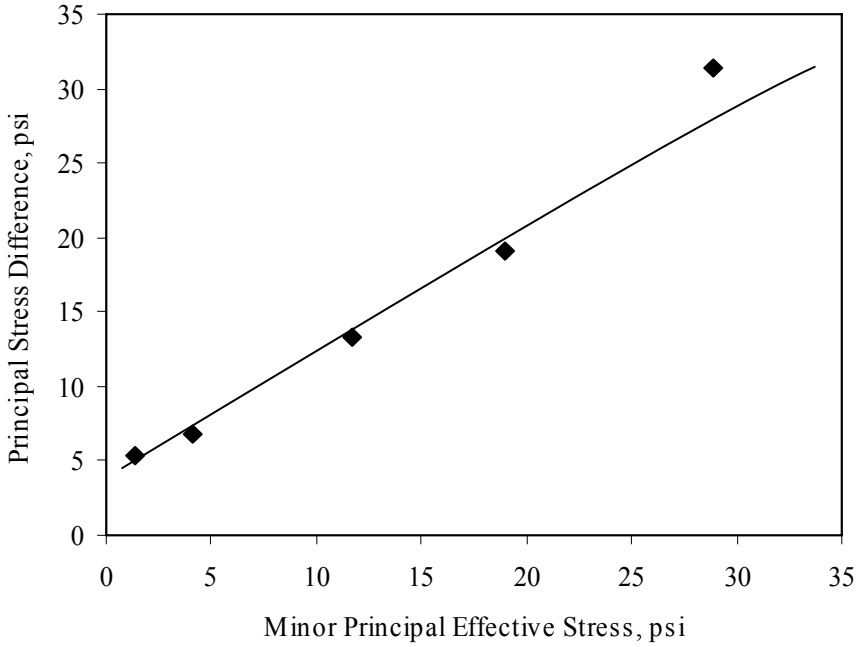

Figure 5.5: Modified Mohr failure envelope for as-compacted specimens of Eagle Ford Shale.

5.4. Specimens Normally Consolidated from a Slurry

Eight consolidated-undrained triaxial compression tests with pore water pressure measurements were performed on specimens normally consolidated from a slurry. The specimens had final effective consolidation pressures of 3 psi to 50 psi. Using effective consolidation pressures less than 2 psi during specimen preparation produced specimens that were too fragile to be handled. Therefore, final effective consolidation pressures less than 3 psi were not used to avoid having the specimens be over-consolidated.

The stress-strain curves in Figure 5.6 show a decrease in stress after the peak principal stress difference was reached. The points where the stress path was approximately tangent to the failure envelope occurred at strains ranging from 1% to 10%. The decrease in stress following failure was more noticeable in specimens consolidated to final effective stresses greater than 25 psi. The two specimens with effective consolidation pressures of 15 psi show very different behavior; one specimen, 15 psi (2), showed a peak principal stress difference at a much lower

strain than the other specimen at the same effective consolidation pressure. Both specimens had B-values of 0.98 prior to consolidation. Figure 5.7 shows that pore water pressures increased in all specimens throughout shear, which is to be expected for normally consolidated soils.

A modified Mohr failure envelope is drawn through the points of failure based on stress path tangency in Figure 5.8. Although there is scatter in the data for the normally consolidated specimens, it appears that the failure envelope is curved at low effective stresses. Had further tests been possible at effective stresses less than 3 psi, the failure envelope would be expected to pass through the origin. A value of zero cohesion is generally expected for normally consolidated clay, unless the soil is cemented.

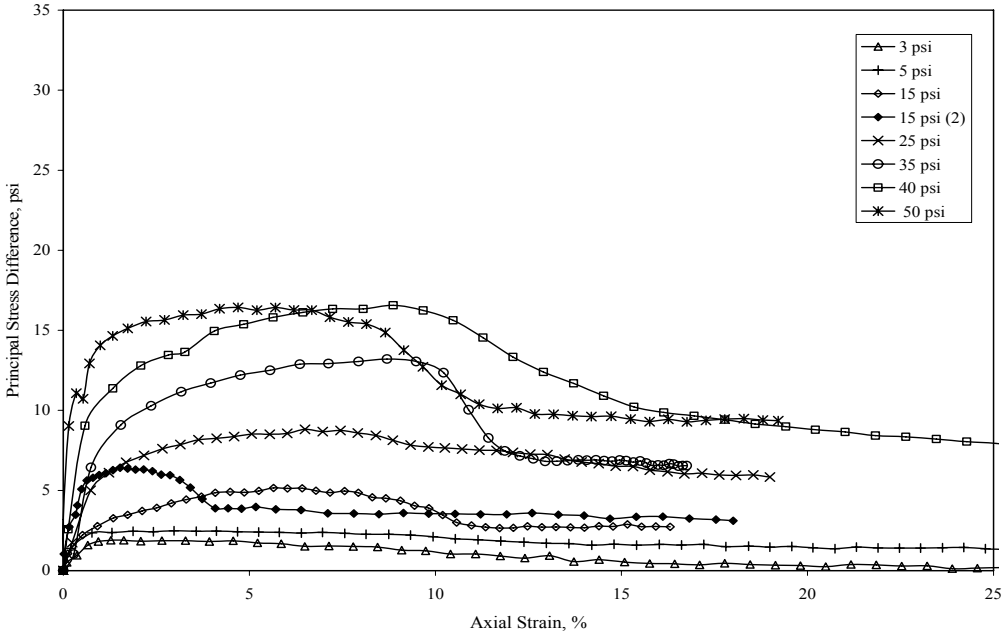

Figure 5.6: Stress-strain curves for Eagle Ford Shale normally consolidated from a slurry

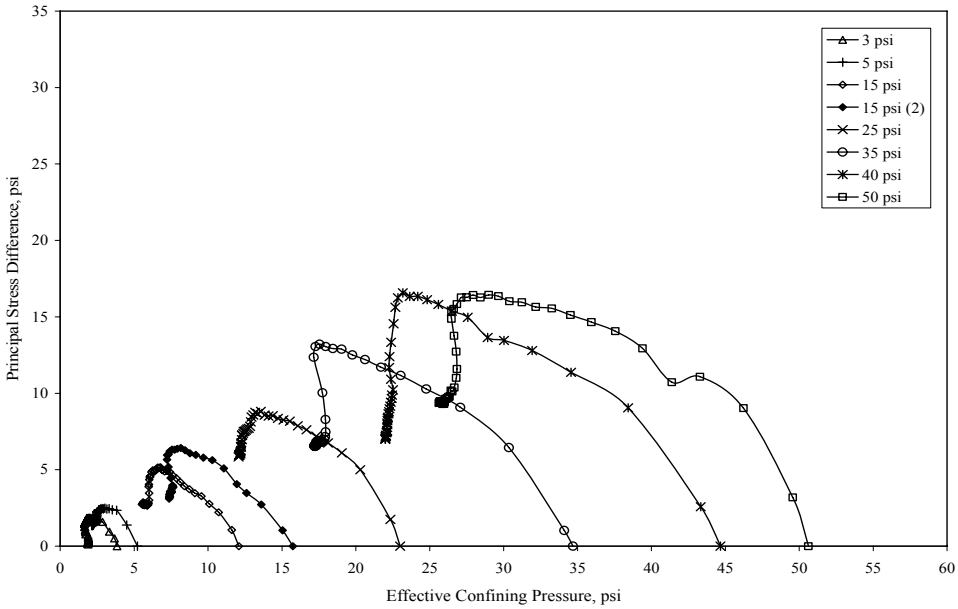

Figure 5.7: Modified Mohr-Coulomb diagram for normally consolidated specimens of Eagle Ford Shale

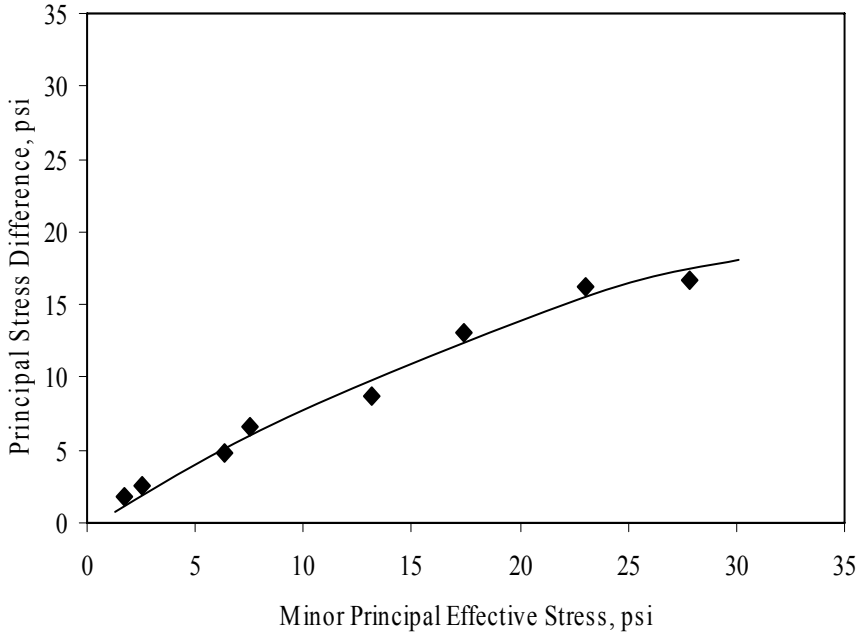

Figure 5.8: Modified Mohr failure envelope for specimens of Eagle Ford Shale normally consolidated from a slurry

5.5. Specimens Subjected to Cyclic Wetting and Drying

Triaxial compression tests with pore water pressure measurements were conducted on nine specimens after they were subjected to twenty cycles of wetting and drying. The specimens were consolidated to final effective stresses ranging from 1 to 50 psi.

The stress-strain curves for specimens subjected to cyclic wetting and drying are presented in Figure 5.9. The stress-strain curve for the specimen with an effective consolidation pressure of 36 psi ends abruptly due to a loss in power during testing. The reduction in principal stress difference with increasing axial strain is more pronounced for specimens with effective confining stresses greater than or equal to 25 psi (Figure 5.7). However, the failure does not appear to be as brittle-like as for the as-compacted specimens. Failure defined by the points where the effective stress paths became approximately tangent to the failure envelope occurred at strains ranging from 4% to 11%.

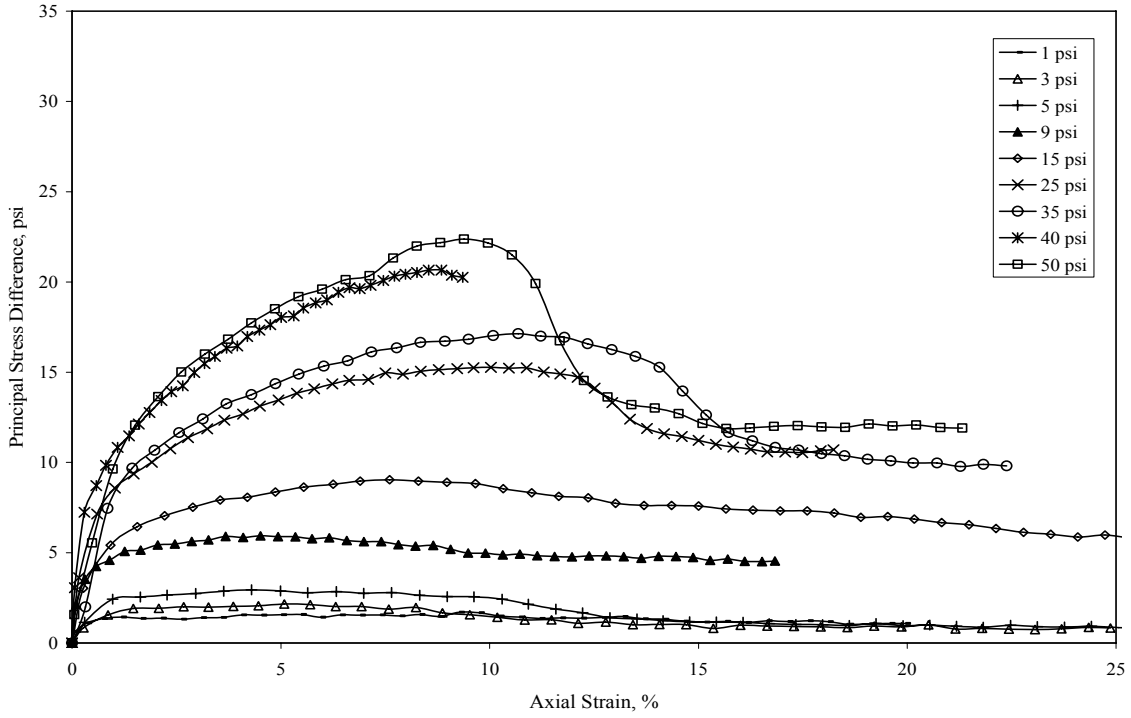

Figure 5.9: Stress-strain curves for specimens of Eagle Ford Shale subjected to cyclic wetting and drying

The effective stress paths and modified Mohr failure envelope are presented in Figures 5.10 and 5.11, respectively. The stress paths for the specimens subjected to cyclic wetting and drying appear very similar to those in Figure 5.5 for the specimens normally consolidated from a slurry. Despite having been compacted, the stresses developed in the specimens subjected to cyclic wetting and drying showed more resemblance to those of the normally consolidated specimens than the as-compacted specimens. The modified Mohr failure envelope shown in Figure 5.9 also shows curvature, and it appears that cohesion is negligible.

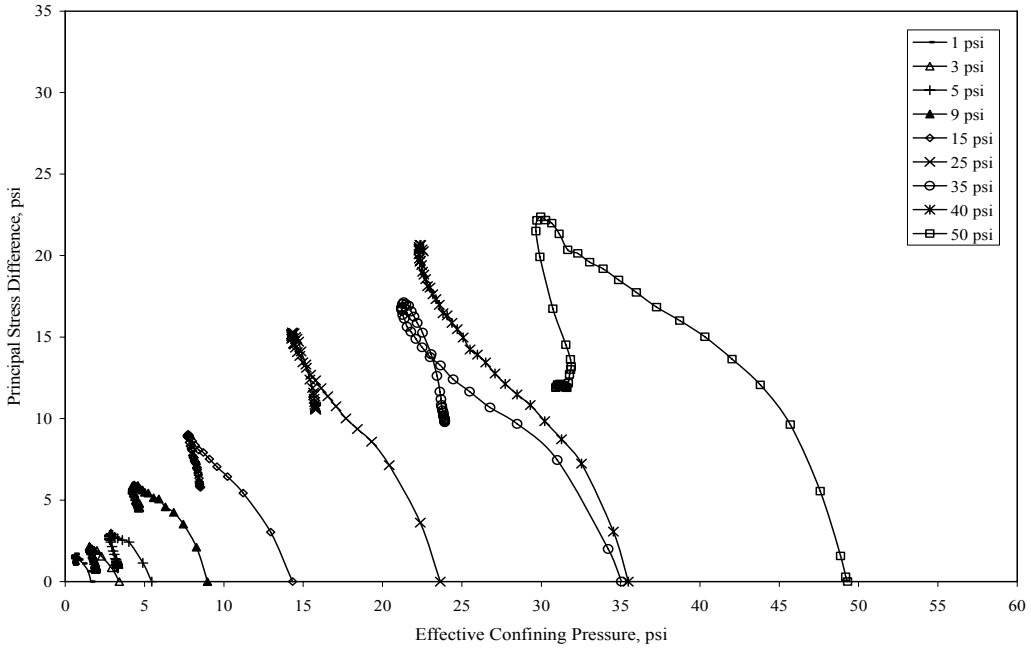

Figure 5.10: Modified Mohr-Coulomb diagram for specimens of Eagle Ford Shale subjected to cyclic wetting and drying

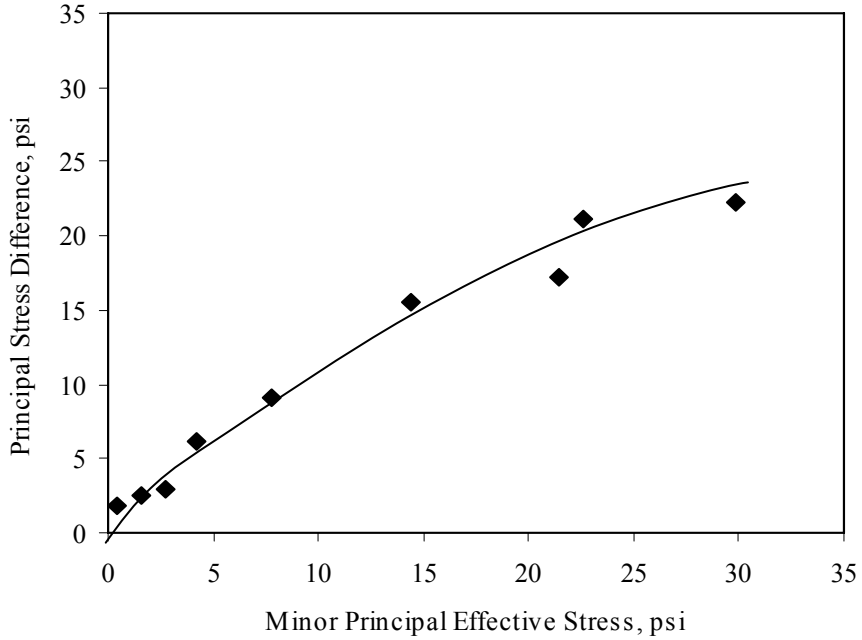

Figure 5.11: Modified Mohr failure envelope for specimens of Eagle Ford Shale subjected to

5.6. Comparison of Shear Strength with Recent Correlations

Wright (2005) developed a correlation equation based on Stark et al.'s (2005) data, where the secant friction angle is related to the logarithm of the effective confining pressure. This is consistent with the following relationship first proposed by Duncan et al. (1989) for cohesionless soil:

$$\varphi'_{secant} = \varphi'_o - \Delta\varphi' \log_{10}\left(\frac{\sigma'_3}{p_a}\right)$$

Equation 7.1

where, φ_o' is the secant friction angle at an effective confining pressure, σ'_3, of one atmosphere, $\Delta\varphi'$ is the change in the secant friction angle with each ten-fold ($\log_{10}$ cycle) increase in confining pressure, and p_a is atmospheric pressure.

The only difference between Equation 7.1, suggested by Duncan et al. (1989), and the equation used by Wright is that the effective normal stress on the failure plane, σ'_f, was used in place of the effective confining pressure, σ'_3. Thus, for Wright's equation,

$$\varphi'_{secant} = \varphi'_o - \Delta\varphi' \log_{10}\left(\frac{\sigma'_f}{p_a}\right)$$

Equation 7.2

Using equation 7.2 and the fully softened secant friction angles from Stark et al. (2005), Wright determined values for φ_o' and $\Delta\varphi'$. Based on these values he proposed, the following relationship between the fully softened secant friction angle and the logarithm of the effective normal stress:

$$\varphi'_{secant} = 55.3° - 16.7° \log_{10}(\omega_{LL}) - 6° \log_{10}\left(\frac{\sigma'_f}{p_a}\right)$$

Equation 7.3

where, ω_{LL} is the liquid limit, and the other parameters are the same as defined above.

The secant friction angles of Eagle Ford Shale for specimens subjected to wetting and drying and those normally consolidated from a slurry are compared with values of the fully softened secant friction angles calculated using Wright's (2005) correlation in Figures 5.12 and 5.13. Wright's correlation appears to be a very good approximation of secant friction angles when for specimens of Eagle Ford Shale subjected to wetting and drying. However, Wright's correlation does not agree well with the data for specimens normally consolidated from a slurry. This is to be expected because Wright's equation was based on Stark et al.'s (2005) data, which also did not agree as well with the data for the normally consolidated specimens.

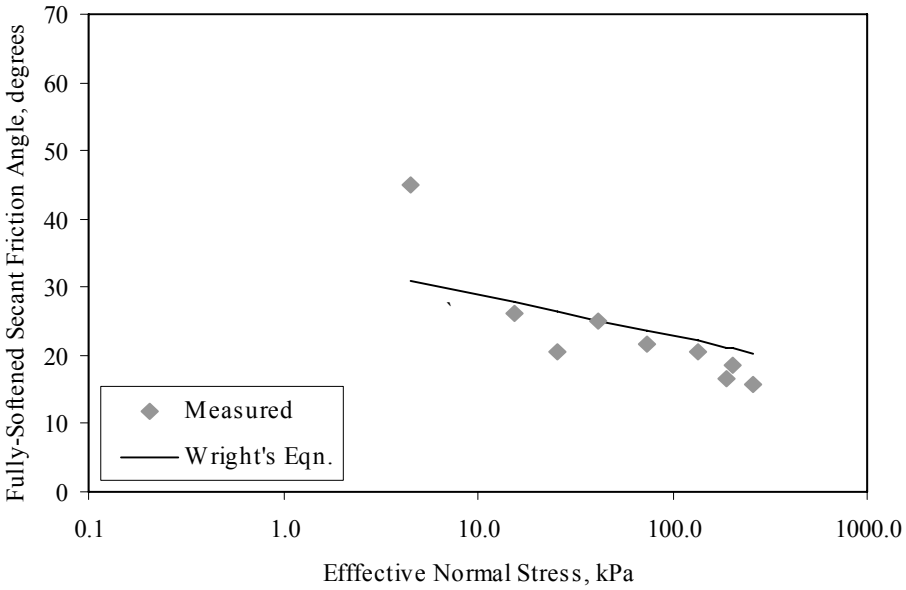

Figure 5.12: Comparison of the fully softened secant friction angles measured and calculated using Wright's (2005) correlation for Eagle Ford Shale subjected to cyclic wetting and drying.

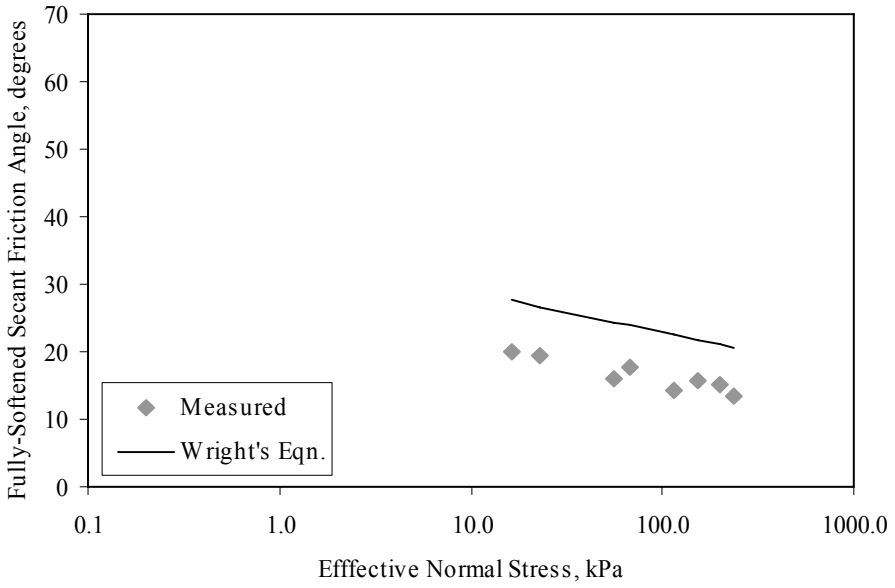

Figure 5.13: Comparison of the fully softened secant friction angles measured and calculated using Wright's (2005) correlation for specimens of Eagle Ford Shale normally consolidated from a slurry.

A comprehensive discussion on the comparison of the shear strength results obtained in this study and other correlations is provided in the companion report 5-9023-3 (Wright and Aguettant 2003). Stark et al.'s (2005) correlation for the fully softened secant friction angle agrees well with the measured fully softened secant friction angles for Eagle Ford Shale, especially for the secant friction angles from the specimens that were subjected to cyclic wetting

and drying. Wright's (2005) correlation also proves to agree well with the measured fully softened secant friction angles for Eagle Ford Shale, as obtained in this study.

Chapter 6. Refined and Calibrated Model for Determination of Suction Profiles in High PI Clay Embankments and Determination of the Depth of Moisture Fluctuations

6.1. Depth of Moisture Fluctuations

An important aspect of this study involves defining the seasonal fluctuations of suction within a soil profile. This section provides a summary of the investigation presented in Appendix A of the companion report 5-9023-2 (Kuhn and Zornberg 2006). The suction fluctuations depend on fluctuations in water content and show decreasing amplitude with increasing depth into a soil profile. At a certain depth, the suction fluctuations will be small enough that they may be considered to have little effect on moisture movements within the soil. This depth can be referred to as the depth of moisture fluctuation. The depth of moisture fluctuations for a generic soil profile is shown in Figure 6.1.

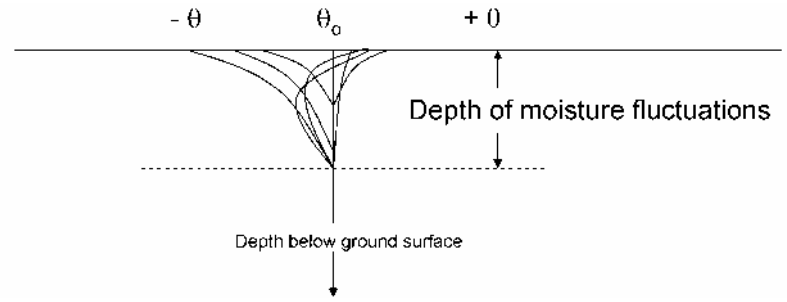

Figure 6.1: Depth of moisture fluctuations within a soil profile

The same suction fluctuations that occur in level ground are expected to be similar to those occurring in slopes. The difference between infiltration into an earthen slope and infiltration into level ground is that runoff will occur in a slope, while ponding may occur in level ground. Assuming a uniform depth of moisture fluctuations along the width of the slope, the zone of moisture fluctuations is represented in Figure 6.2. As noted in Figure 6.2, the soil below the zone of moisture fluctuations is likely intact because it has not been exposed to significant cycles of wetting and drying.

The moisture fluctuations can result in a discontinuity in shear strength and hydraulic characteristics at that particular depth. The variation in hydraulic properties between intact clay and clay subjected to cycles of wetting and drying was evaluated in section 4 of this report. The variation in shear strength between intact clay and clay subjected to cycles of wetting and drying was evaluated in section 5 of this report.

The depth of moisture fluctuation is investigated in this section, as it is expected to define the two regions in a slope with different shear strength and hydraulic properties. The estimated depth of moisture fluctuations can be subsequently used in slope stability analyses.

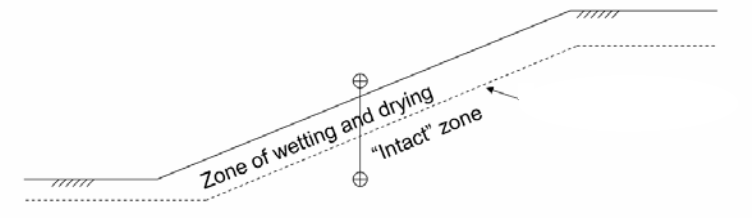

Figure 6.2: Depth of moisture fluctuations within a soil slope

6.2. Modeling Procedure

The depth of moisture fluctuations in cracked high PI clay was analyzed using the finite element flow program SVflux (SoilVision Systems Ltd., Saskatoon, Canada). SVflux is a component of the software suite SoilVision. For the analysis, a one-dimensional finite element flow model with a 6-meter profile was used. The top boundary of the model was specified as a flux boundary where temperature, precipitation, potential evapotranspiration, and relative humidity were input in order to determine the flux through the surface of the soil profile. Simulations were conducted using weather records representative of both Austin and Houston, as these are the locations where comprehensive shear strength information for high PI clays is available. Records of temperature, precipitation, and potential evaporation for Austin and Houston were obtained from the Texas Evapotranspiration Network, as shown for the year 2003 in Figures 6.3, 6.4, and 6.5. The average quarterly relative humidity values for Austin and Houston were obtained using the HELP model (Table 6.1). The bottom boundary was specified as a seepage face boundary condition and was located 6 meters below the upper boundary as to minimize its effect on the moisture fluctuations at shallow depths.

Simulations using weather conditions for both Austin and Houston were used. Records of temperature, precipitation, and potential evapotranspiration for Austin and Houston were obtained from the Texas Evapotranspiration Network, as shown in Figures 6.3, 6.4, and 6.5. The average quarterly values of relative humidity for Austin and Houston were obtained from the HELP model and are shown in Table 6.1. The bottom boundary was specified as a seepage face boundary condition and was placed 6 meters below the upper boundary as to not effect moisture fluctuations at shallow depths.

The finite element flow model for Austin and Houston weather conditions and the aforementioned hydraulic properties of cracked high PI clay was run for a simulation time of 30 years. The model was run twice for each city, once without accounting for runoff and once accounting for runoff. At the beginning of the simulation, a suction of 10 kPa was specified for the 6-meter-profile. By the end of the 30-year simulation, an annual pattern of suction and volumetric water content profile changes with time was established using the input weather and hydraulic parameters. This pattern of suction and water content profile change is used in the subsequent analysis to determine the depth of moisture fluctuation.

The two components of the SoilVision suite that were used in this analysis are SVFlux and FlexPDE. SVflux is used to create the finite element mesh and input the boundary conditions and output parameters while FlexPDE is used to solve the partial differential equation for the flow of water through unsaturated soil.

Table 6.1: Average quarterly values of relative humidity for Austin and Houston

Quarter	Austin Relative humidity (%)	Houston relative humidity (%)
1st	66	74
2nd	70	76
3rd	66	77
4th	67	77

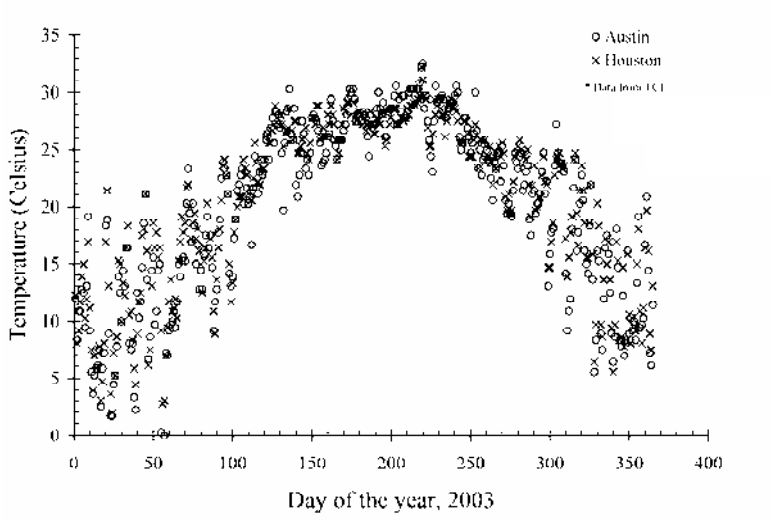

Figure 6.3: Daily temperate inputs for Austin and Houston simulations

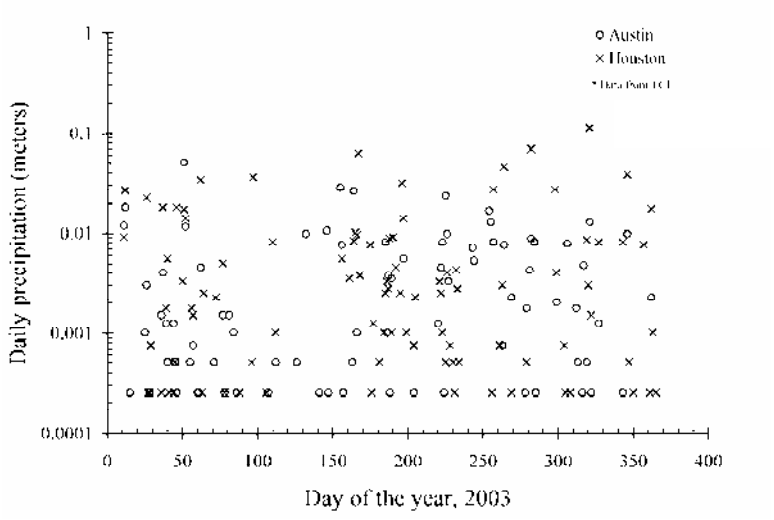

Figure 6.4: Daily precipitation inputs for Austin and Houston simulations

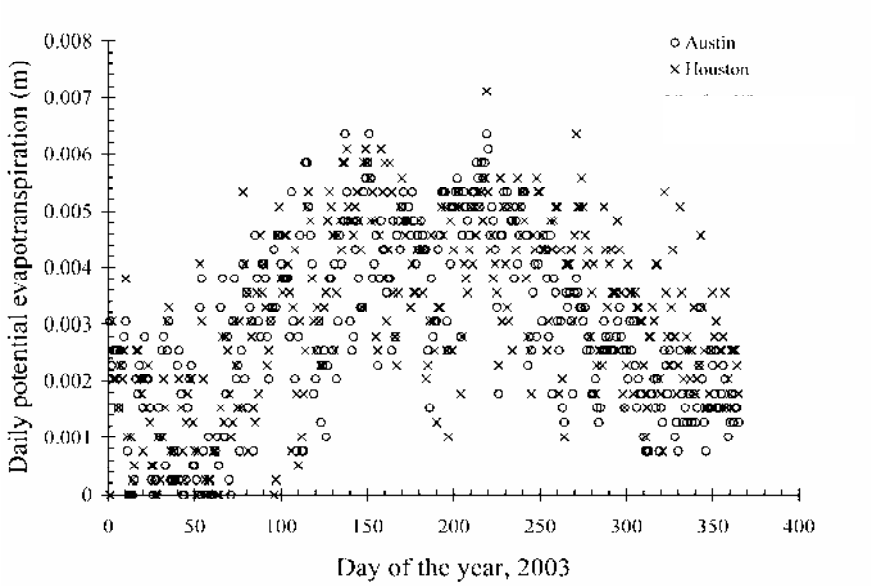

Figure 6.5: Daily potential evaporation inputs for Austin and Houston simulations

6.3. Predicted Field Suction Profiles

The 30-year simulation for weather conditions of Austin and Houston allowed determination of the annual pattern of moisture and suction profiles. The values of moisture content and suction throughout the multiple years in the simulation can be found in Figures 6.6 and 6.7 for the first 3 meters of the modeled profile using Austin weather conditions. The variations in moisture and suction profiles for Houston weather condition are shown in Figures 6.7 and 6.8. The light curves in these figures represent bi-monthly moisture and suction profiles modeled for Austin and Houston. The darker lines represent the lower bound, median, and upper bound values of volumetric water content and suction modeled for Austin and Houston.

In order to evaluate the effect of incorporating runoff into the model, simulations were conducted for both Austin and Houston conditions accounting for runoff. For Austin, the resulting variation of the volumetric water content profile was not significantly different from the simulation that did not account for runoff. For Houston, however, the resulting variation of the volumetric moisture content profile was similar in shape but was shifted to the left, as shown in Figure 6.10. When suction profiles are compared for Houston modeled with and without runoff, the suctions predicted with runoff are greater than those predicted without runoff. In order to not over predict values of field suction, the Houston model without runoff will be used in further evaluations in this study.

Based on the results of the analysis, it appears as though the depth of moisture fluctuations ranges from 1 to 1.5 meters of depth. The depth of moisture fluctuations may be seen in Figure 6.10, which compared moisture content profiles in Austin and Houston. From this figure, it is apparent that there is a zone with distinctly higher volumetric water contents beginning at approximately 1.1 meters of depth. This zone is also apparent for Houston but is not as severe. Accordingly, a depth of moisture fluctuation of 1.1 meters is defined as representative of the depth of moisture fluctuations for both Austin and Houston for a high PI clay with the hydraulic characteristics of Eagle Ford clay. This is consistent with the depth of reported failures in Eagle Ford clay slopes (Kelly 2006).

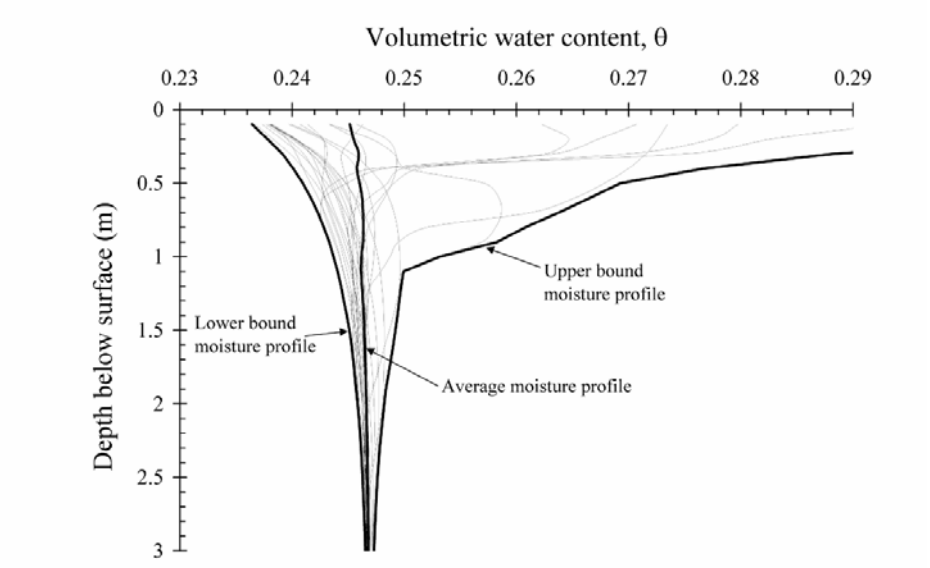

Figure 6.6: Predicted variation of volumetric water content profile over the course of a year for Eagle Ford clay under Austin, TX weather conditions

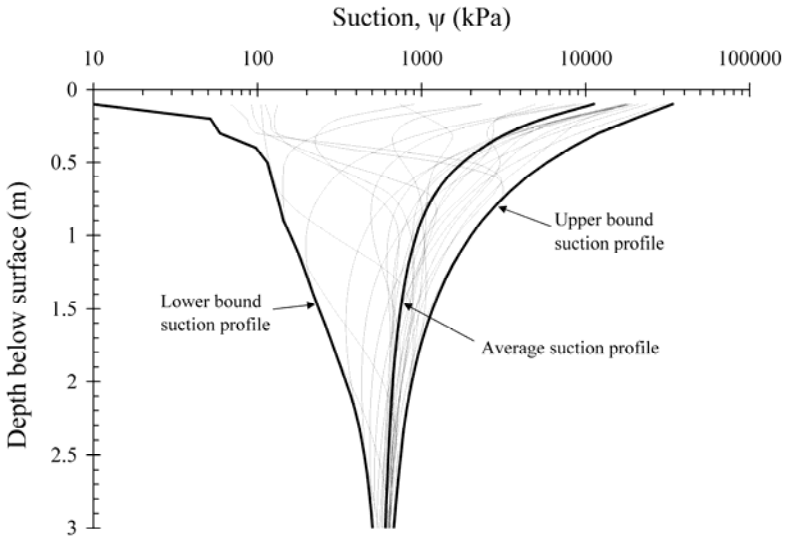

Figure 6.7: Predicted variation of suction profile over the course of a year for Eagle Ford clay under Austin, TX weather conditions

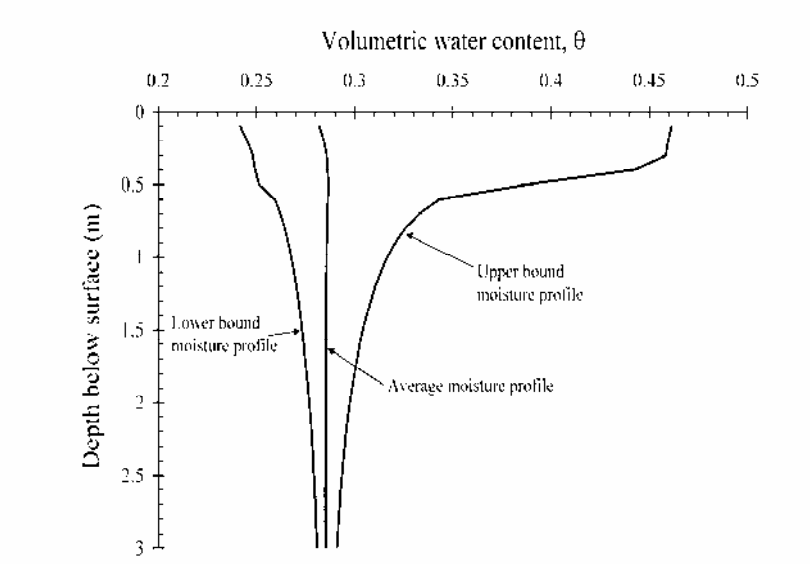

Figure 6.8: Predicted variation of volumetric water content profile over the course of a year for Eagle Ford clay under Houston, TX weather conditions

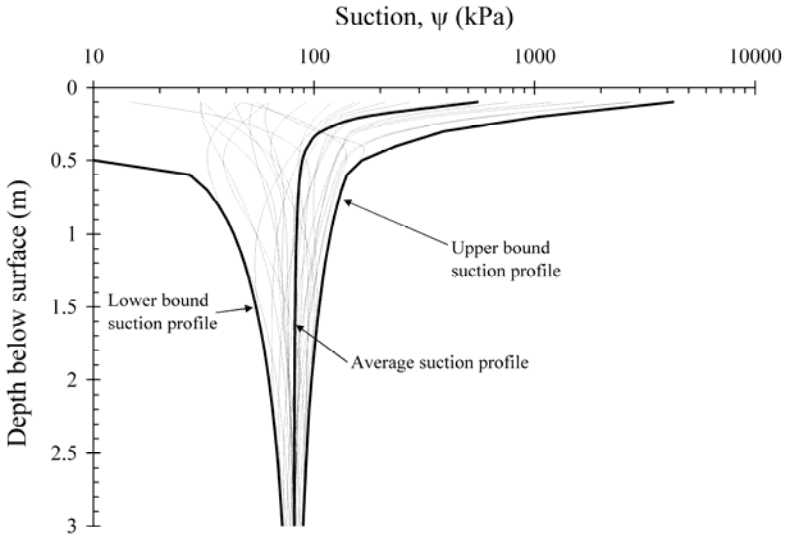

Figure 6.9: Predicted variation of suction profile over the course of a year for Eagle Ford clay under Houston, TX weather conditions

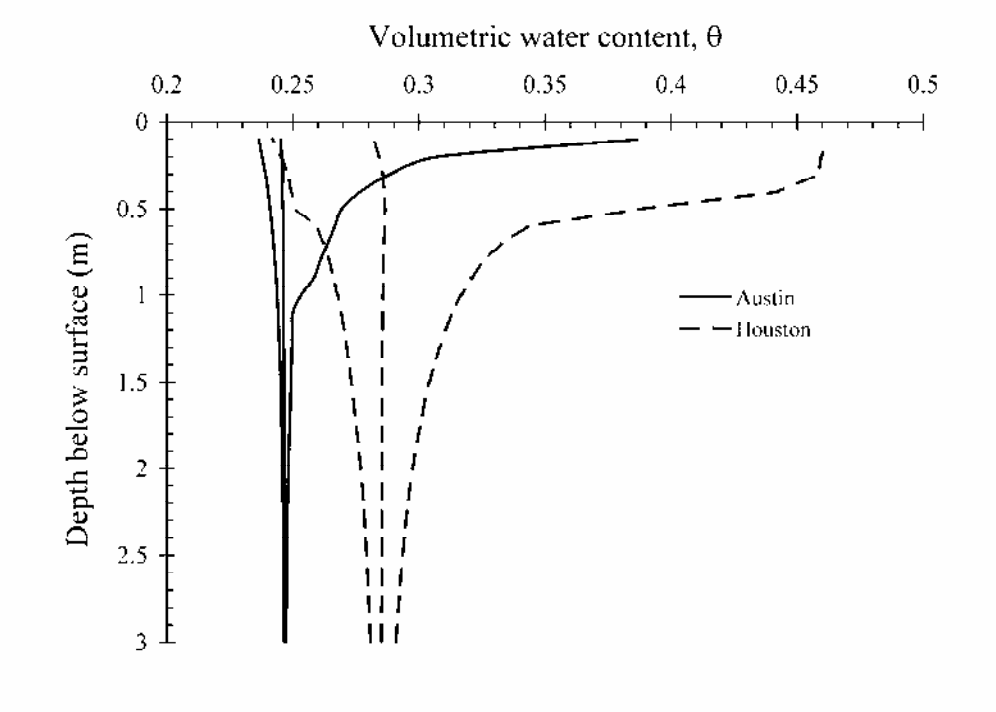

Figure 6.10: Predicted variation of volumetric water content profile over the course of a year for Eagle Ford clay under Austin, TX and Houston, TX weather conditions

Chapter 7. Stability Assessment of High PI Clay Slopes

7.1. Two-Dimensional Slope Stability Analysis

The companion report 5-9023-3 (Wright and Aguettant 2006) presents a series of slope stability calculations performed for the slope in Eagle Ford Shale, where the soil used in this study was obtained. The purpose of these computations was to determine the probable shear strength properties and pore water pressures at the time of failure. The slope has an overall height of 21 ft. The grade gradually increased towards the crest of the slope, as shown in Figure 7.1. Near the crest of the slope, the inclination was approximately 18° from the horizontal, which is approximately a 3:1 slope.

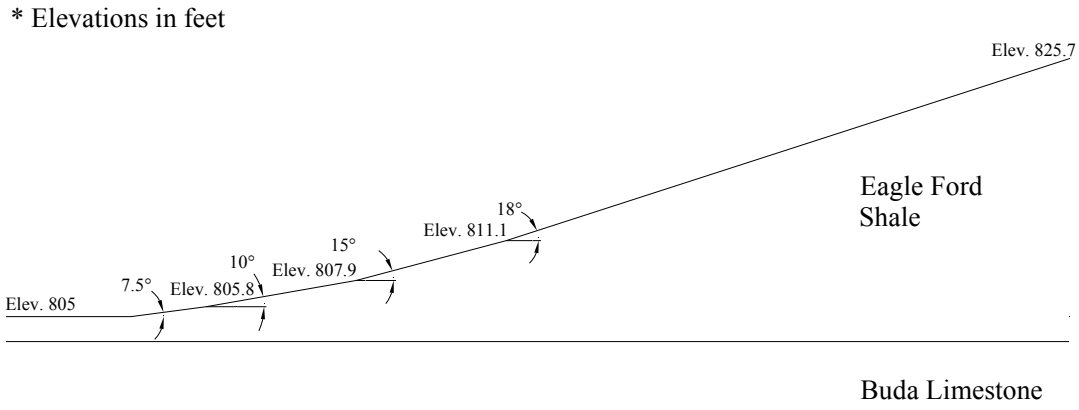

Figure 7.1: Slope geometry used during stability analyses.

The stability analyses were conducted using UTEXAS4 (Wright 2006) to perform an automatic search for the critical circle. Spencer's method was used to calculate the factor of safety. The slope was considered to consist of homogeneous Eagle Ford Shale, underlain by Buda Limestone at a depth of approximately 2 ft below the toe of the slope. Stability analyses were performed using three different representations of shear strength: the as-compacted strength, Fully softened strength (represented by the strength after wetting and drying), and the residual strength.

One of the several series of slope stability calculations was performed using the shear strength envelope for specimens subjected to cyclic wetting and drying. In order to represent the actual slip surface in the field, a set of slope stability calculations was performed where the slip surface was constrained to within the toe and the crest of the slope. These calculations revealed a value of 0.43 for r_u was required to produce a factor of safety of 1.00 (Figure 7.2).

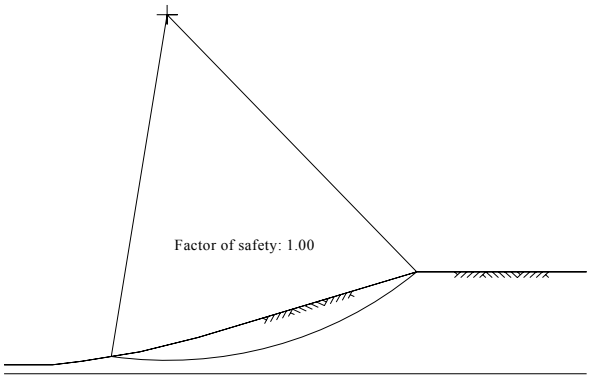

Figure 7.2: Critical circle using the strength after wetting and drying with the slip surface restricted to the slope face (r_u = 0.43)

As shown in Figure 7.1, the upper part of the slope is inclined at an angle of 18° with the horizontal. It seems more likely that failure would occur in this portion of the slope because it has the steepest inclination. Therefore, another set of stability calculations was performed with the slip surface constrained to occur within just the upper, steepest portion of the slope. Under these conditions, a value of 0.53 for r_u was required to produce a factor of safety of 1.00 (Figure 7.3).

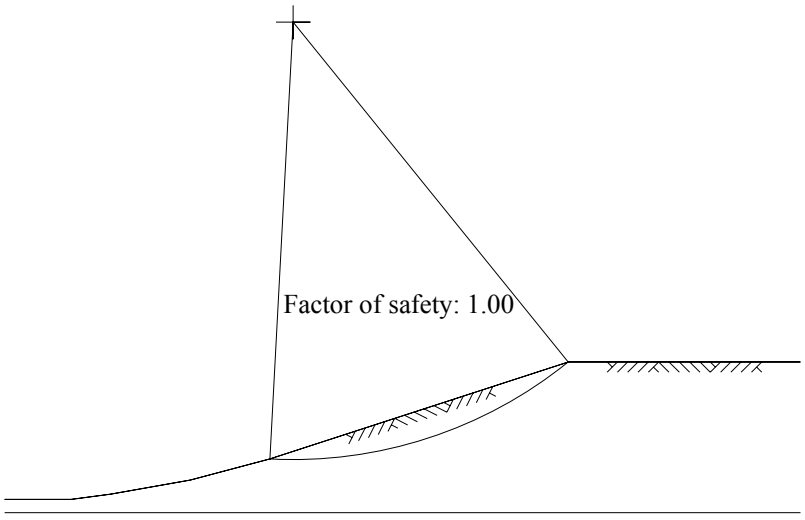

Figure 7.3: Critical circle using the strength after wetting and drying with the slip surface restricted to the upper, steepest part of the slope (r_u = 0.53)

Based on these analyses using the shear strength after wetting and drying, it appears that the pore water pressures present at the time of failure agree well with each other, even for the analyses in which the slip surface is restricted to occur within the slope. The positions of the slip surfaces on the slope are also closer to the actual position of the slip surface in the field than the position of the slip surface when it was not constrained to the slope face. From the analyses with constraints on the position of the slip surface, it appears that the pore water pressure ratio must have been between 0.43 and 0.53 for failure to occur at the fully softened strength condition.

7.2. One-Dimensional Slope Stability Analysis

A series of limit equilibrium infinite slope analysis were conducted using shear strength parameters measured as part of this study, as reported in Appendix B of the companion report 5-9023-2 (Kuhn and Zornberg 2006) .

The infinite slope analyses were conducted for a series of slope angles considering failure depths ranging from 1 to 6 meters. For example, for a slope of and a failure depth for a slope of 18^0 and a failure depth of 1.1 meter in weathered Eagle Ford clay, a pore water pressure of 6.5 kPa is needed to produce a factor of safety of 1.0 in an infinite slope analysis. Different representative values of pore water pressure were used until a factor of safety of 1.0 was achieved. The shear strength used for the analysis was determined using the relationship presented in section 5.6 of this report. In order to use this relationship, the effective stress must be input for the depth of failure. For this case, the total stress was calculated and the pore water pressure was varied in order to produce a factor of safety of 1.0. The results of the analysis are shown in Figure 7.4. The values of pore water pressure determined from the analysis reveal that the pore water pressure at failure should be positive (in excess of atmospheric pressure) in order to reach failure in slope with a cotangent slope angle of greater than 2.5 for Eagle Ford Clay. Additional analyses indicate that a positive pore water pressure are needed for failing slopes in Paris clay with cotangents greater than 2.0 and for slopes in Beaumont clay with cotangents over 1.5.

In order to compare this example calculation with the results of the limit equilibrium circular clip surface analysis presented in section 7.1 of this report, the pore water pressure can be expressed in terms of the pore water pressure ratio. The pore water pressure ratio, r_u, is the ratio of the pore water pressure to the total stress at the point of interest. Using the aforementioned example of a 18^0 slope with a depth of failure of 1.1 meters leads to a pore water pressure ratio of 0.34. The pore water pressure ratio reported in section 7.1 of this report considering circular slip surfaces ranged between 0.5 and 0.6 (see also Wright and Aguettant, TxDOT report 0-5202-3). The range in pore water pressure ratio suggested by Wright and Aguettant is plotted along with the pore water pressure ratio calculated from an infinite slope analysis for the shear strength properties of weathered Eagle Ford clay in Figure 7.5.

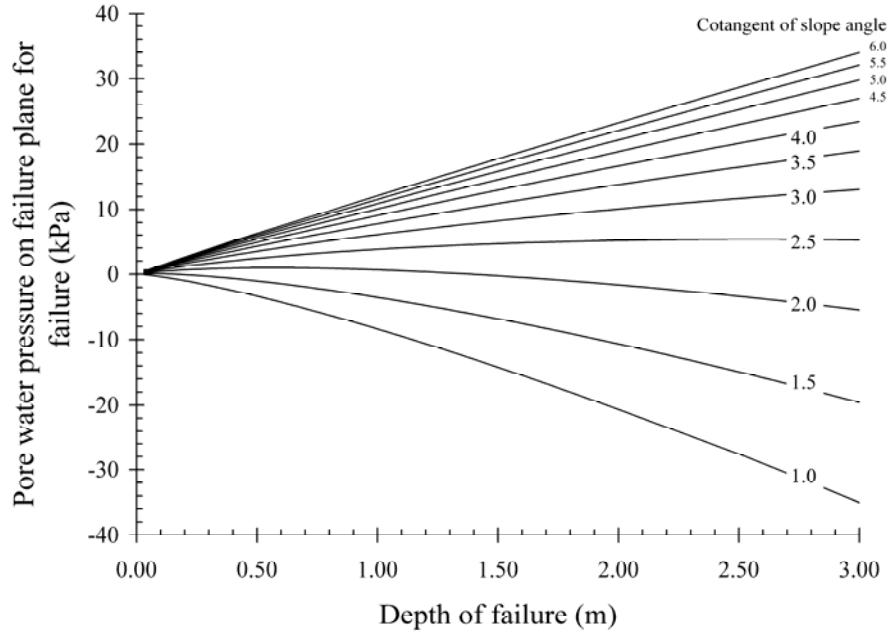

Figure 7.4: Back calculated pore water pressure at failure using the secant friction angle for weathered Eagle Ford clay

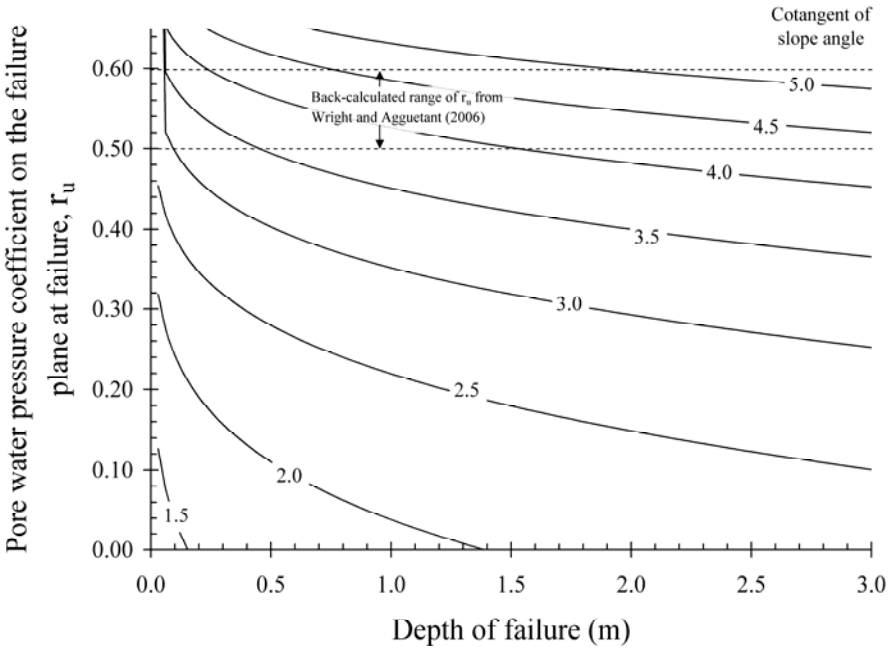

Figure 7.5: Back calculated pore water pressure coefficients at failure using the secant friction angle for weathered Eagle Ford clay

In addition to calculating the pore water pressure on the failure plane for conditions of failure for a range of slope angles and failure depths, the maximum possible slope angle under conditions of seepage parallel to the slope face was calculated using different failure depths. The resulting relationship between the maximum slope angle and the depth of the failure plane for conditions of seepage parallel to the slope face is shown in Figure 7.6. This relationship was

obtained by solving a set of two nonlinear equations representing the pore water pressure on the failure plane due to seepage and limit equilibrium conditions for an infinite slope. For the example case of a failure depth of 1.1 meters in Eagle Ford clay, a slope of 4.1:1 would lead to a factor of safety of 1.0 for an infinite slope analysis assuming seepage parallel to the slope face. The pore water pressure on the failure plane at failure associated with a failure depth of 1.1 meters for each of the soils is presented in Figure 7.7. These pore water pressures were used to evaluate the recurrence rate of failures for a depth of moisture fluctuation of 1.1 meters (Kuhn and Zornberg 2006).

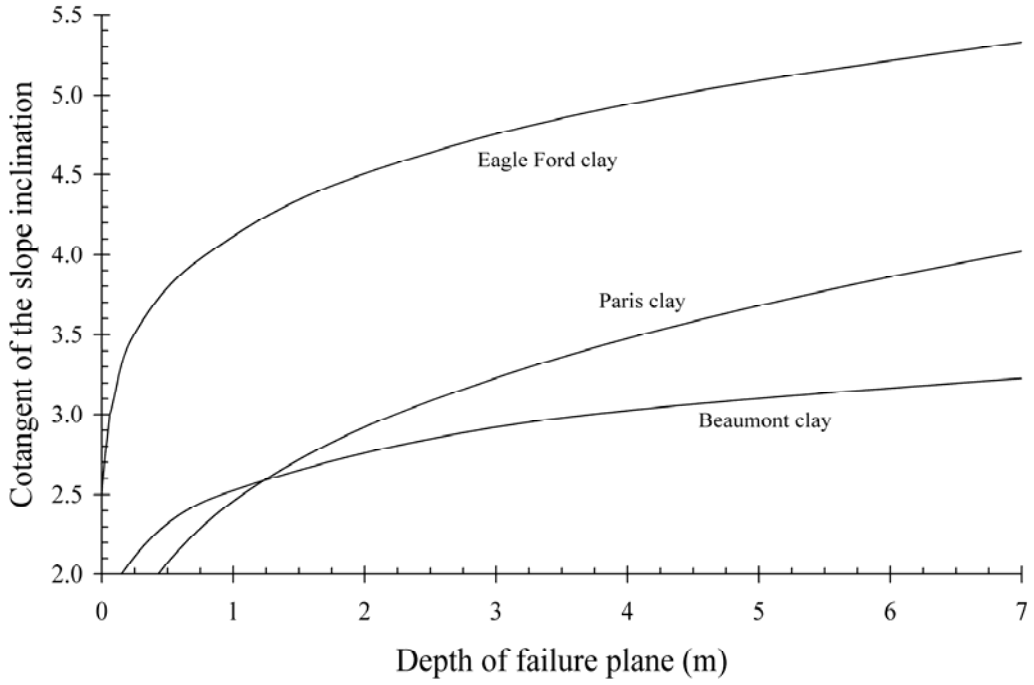

Figure 7.6: Slope inclination for a given failure depth for conditions for limit equilibrium for infinite slope with flow parallel to the slope surface

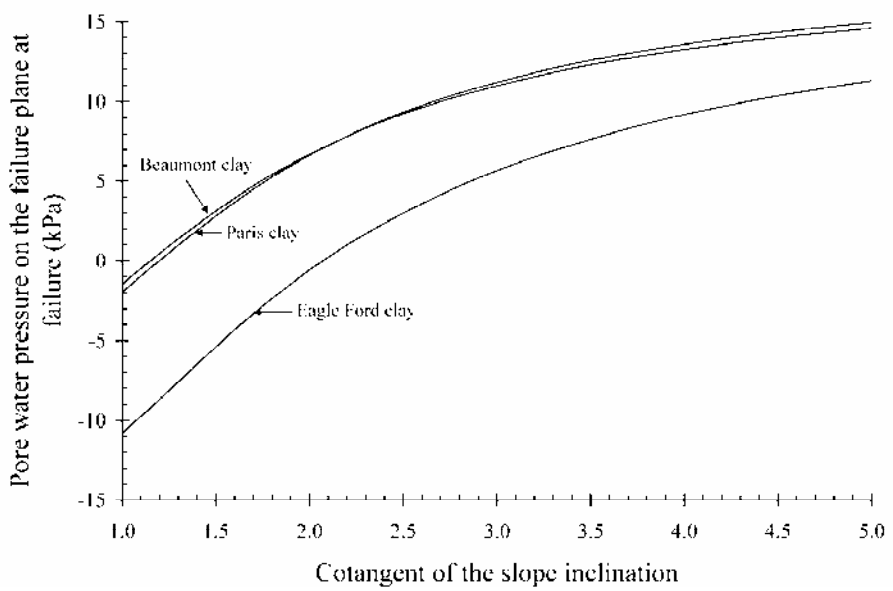

Figure 7.7: Pore water pressure on the failure plane at failure for an assumed failure depth of 1.1 meters

7.3. Discussion

From the slope stability analyses conducted in this study, it appears that the fully softened shear strength, represented by the strength of specimens after cyclic wetting and drying, best represents the strength of the Eagle Ford Shale at the time the slope failed. Also, the pore water pressures would have to be reasonably large to cause failure. The pore water pressure ratio (r_u) required to cause failure should range from 0.43 to 0.53. This corresponds to pore water pressures almost as high as for steady-state horizontal seepage near the face of the slope. Kayyal and Wright (1991) similarly concluded from their slope stability analyses of embankments of Paris and Beaumont clay that using the strength from specimens that were subjected to wetting and drying produced factors of safety of 1.00 with r_u = 0.5 to 0.6.

Aubeny and Lytton (2004) suggested that negative pore water pressures, or suction, may be relied upon for strength in compacted slopes of high plasticity clay that have been exposed to seasonal wetting and drying. They reported that failure is triggered by moisture diffusion and loss of suction with time. However, as has been shown for slopes in Eagle Ford Shale, Paris clay, and Beaumont clay, positive pore water pressures must be present for failure to occur.

The shear strength of the soil in the slope at the time of failure appears to have been much less than the as-compacted strength, yet greater than the residual strength. For the as-compacted strength to be applicable, extremely large positive pore water pressures would be necessary to cause failure.

One dimensional stability analyses were also conducted to evaluate the possible scenario of seepage parallel to the slope face, a condition often considered the worst case scenario. Overall, the infinite slope limit equilibrium stability analyses conducted as part of this study indicate that positive pore water pressures are required to induce failure in a typical high PI clay slope (e.g., 4:1 slopes). Effective shear strength properties from fully softened specimens are recommended for these analyses.

Chapter 8. Site Visits Involving Failure in High PI Clay

A number of field visits were conducted as part of this study in order to evaluate the mechanisms leading to slope failures in compacted embankments of high PI clay. A description of the field observations is provided in Appendix D of the companion report 5-9023-2 (Kuhn and Zornberg 2006). In addition to documenting the slope failures at these sites, the field visits have provided the opportunity to interview TxDOT employees concerning details on the failures. The sites that have been visited as part of this study are summarized in Table 8.1.

Table 8.1: Site visits

	Site	Cut or fill	Remedial efforts	Date of visit	TxDOT contact
1	Hester's Crossing, Williamson County, TX	cut	Plans for an MSE wall	10/15/2004	Marcus Galvan
2	183 & Boggy Creek, Travis County, TX	cut	Plans for a gabion tie-back wall	03/03/2005	Marcus Galvan
3	183 and MLK, Travis County, TX	cut	None so far	03/08/2005	Marcus Galvan
4	IH 30 in Fort Worth Tarrant County, TX	cut/fill	Tire Bales	04/07/2005	Richard Williammee
5	SH 6 and SH 105 Travis County, TX	fill	Fiber Reinforcement	05/25/2005	Darlene Goehl
6	SH & Little Brazos River, Brazos County, TX	fill	Backfill with granular material	02/16/2006	Darlene Goehl

Details of each site visit are provided in the companion report and are not repeated here. Sites visited have included both cuts and fills in high PI clay. Remedial efforts that have been planned and or carried out are also documented.

Chapter 9. Assessment of Surface Conditions and Drain Installations

This section provides an assessment of surface conditions by evaluating the recurrence of slope failures of compacted highly plastic clay if the slope failures remain exposed. The consequences of exposed surface on shear strength, cracking, and hydraulic properties are significant. Consequently, surface treatments aimed at minimizing the effect of wetting and drying will result in improved stability. Since cycles of positive pore water pressures have been shown to contribute to the instability of slopes, the use of toe drains should be considered as part of the design of slopes in high PI clays. The comprehensive experimental data collected on the shear strength and hydraulic properties of Eagle Ford Clay allowed for a preliminary assessment of the recurrence of precipitation events that would trigger failures on embankments of high PI clays in cases where the slope surface remains exposed and toe drains are not used. This section summarizes the results provided in Appendix D of the companion report 5-9023-2 (Kuhn and Zornberg).

This preliminary evaluation considers the shear strength and hydraulic properties determined in the laboratory for long-term conditions (after cycles of wetting and drying). The proposed model to relate moisture infiltration and pore water pressures obtained for a discrete precipitation event is shown in Figure 9.1. For this model, the depth of the moisture fluctuations is assumed as the depth where positive pore water pressures will develop (due to contrasting hydraulic properties between intact and fissured clay). The moisture conditions of the soil before the precipitation event is assumed to be defined by the mean moisture content determined in Section 6. Specifically, the equilibrium moisture content for Eagle Ford clay under Austin weather conditions is approximately 0.25. The moisture condition under failure conditions is assumed to involve the full saturation up to a critical elevation of water table above the depth of moisture fluctuations. The critical elevation is defined by the pore water pressure required for failure of an infinite slope (Section 7), while the assumptions of moisture conditions before the precipitation event and at the moment of failure require additional validation; they are adopted in this study for preliminary evaluation of the recurrence of failure. Additional discussion on the determination of the amount of precipitation needed to induce changes in moisture form the initial to the failure conditions are provided in the companion report 5-9023-02 (Kuhn and Zornberg 2006).

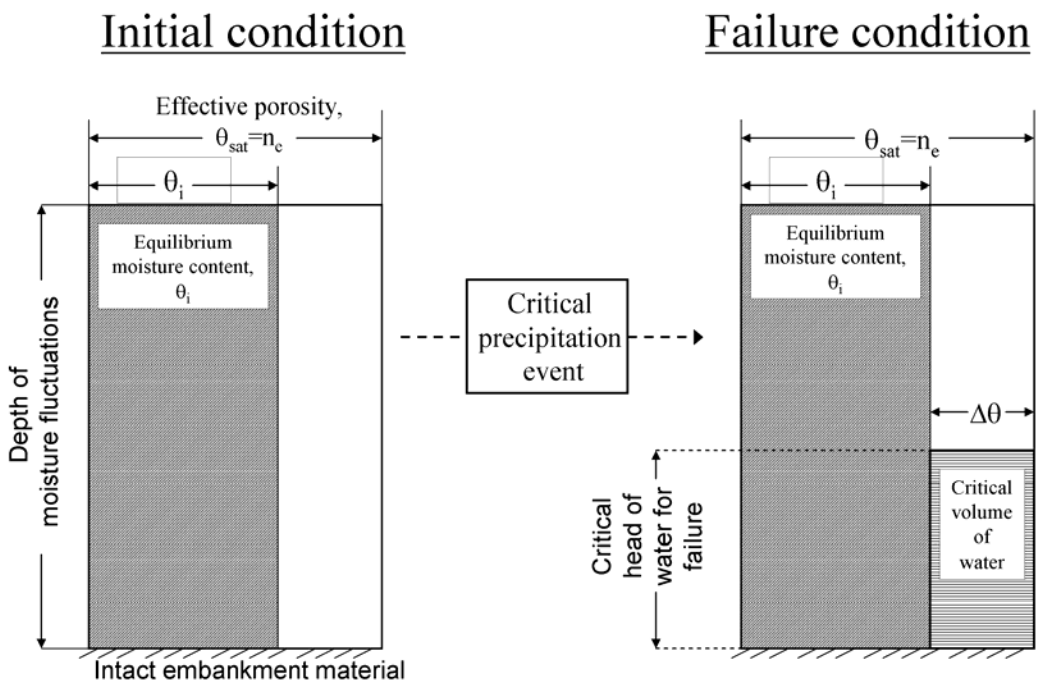

Figure 9.1: Model for failure under discrete precipitation events

In order to determine the recurrence of failure for a given high PI clay slope under a discrete rainfall event, the intensity, duration, and frequency of rainfall events must be considered. The rainfall intensity-duration-frequency (IDF) relationship for Austin, Texas reported by McKinney (2006) is shown in Figure 9.2. The IDF relationship can be used to evaluate the recurrence of shallow slope failures in high PI clay. This requires the shear strength parameters for Eagle Ford Clay (Equation 7.3), the mean volumetric water content profile obtained in the depth of moisture fluctuation analysis (Figure 6.6), and the pore water pressure required to cause failure for a given slope angle at a failure depth of 1.1 meters (Figure 7.7). With this information, a relationship between the cotangent of the slope angle and the combined intensity and duration required to cause failure was obtained (Figure 9.3). For this analysis, the rainfall intensity is assumed equal the infiltration. This infiltration corresponds to the worst-case scenario because any runoff would reduce the amount of infiltration for a given precipitation event. The runoff, however, would be less significant for low intensity, long duration events than for high intensity, short duration events.

This relationship can also be presented in terms of storm duration and storm intensity, as shown in Figures 9.4 and 9.5, respectively. Both charts were established for rainfall durations below 100 minutes. Considering that the infiltration rate approaches the precipitation rate for longer durations (i.e., 100 minute events), the cumulative infiltration is shown in Figure 9.6, assuming no runoff. Considering long rainfall durations (100 minutes), failure under a discrete event for a slope of 3.0:1 has a mean recurrence rate of approximately 30 years, according to this evaluation. This is consistent with reported failures of embankments in high PI clays (Kayyal and Wright 1991). While this analysis is preliminary, it provides a rational method to explain the failure in high PI clays. Failure is a consequence of large precipitation events with a certain recurrence (leading to positive pore water pressure) and not a consequence of decreasing suction

due to diffusion processes (leading to a still negative pore water pressure at the moment of failure).

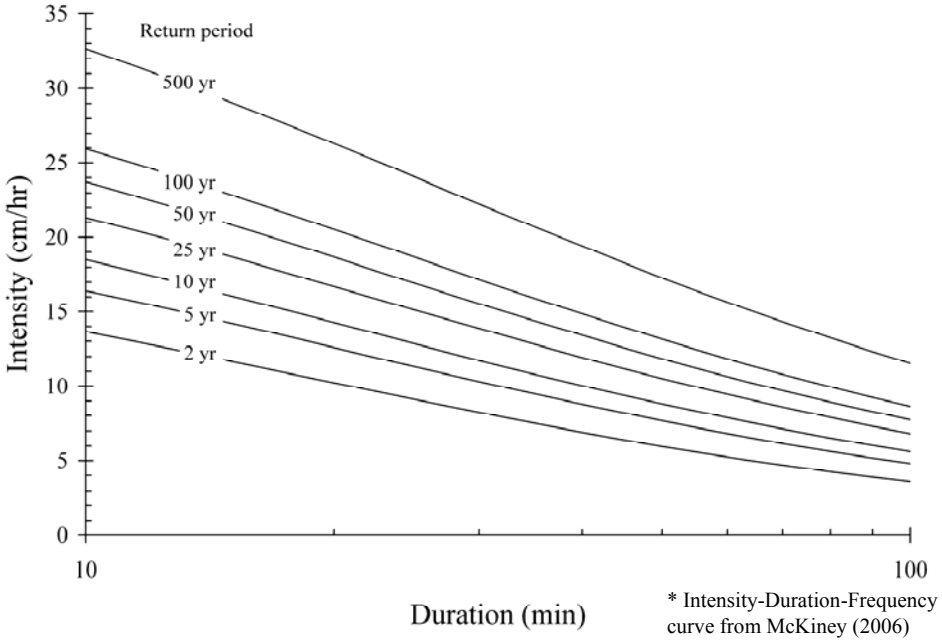

Figure 9.2: Rainfall intensity-duration-frequency curve for Austin, TX

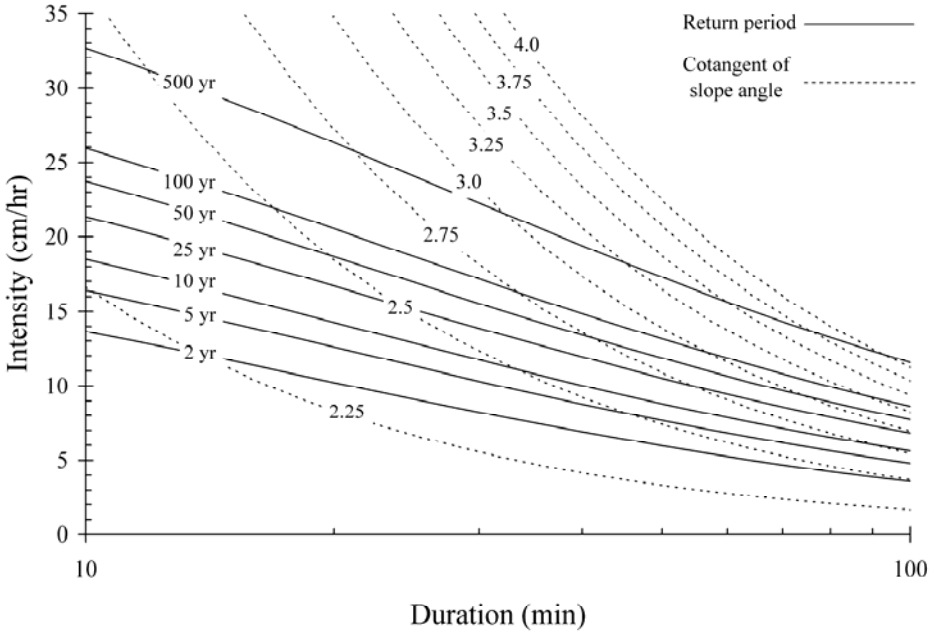

Figure 9.3: Recurrence rate of failures for cracked Eagle Ford clay under Austin weather conditions given a failure depth of 1.1 meters

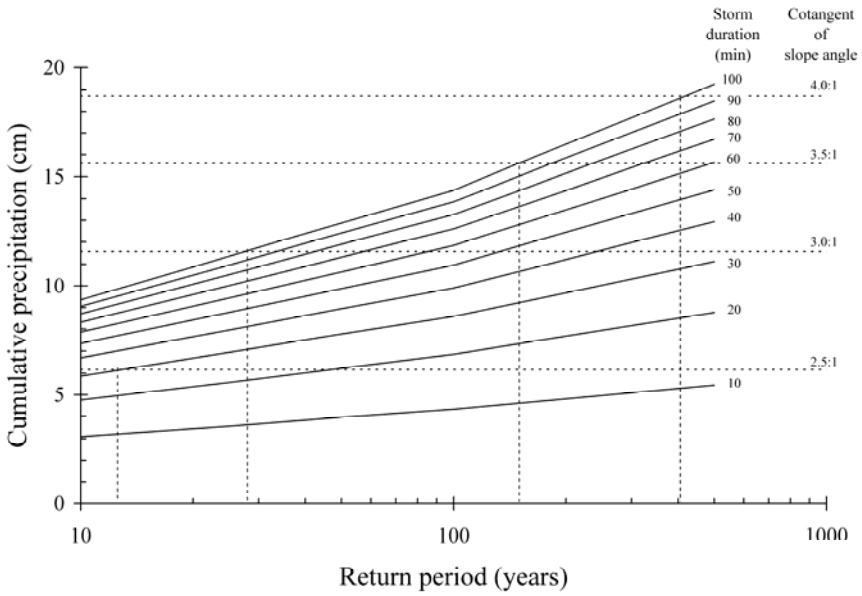

Figure 9.4: Recurrence rate of failures for cracked Eagle Ford clay under Austin weather conditions given a failure depth of 1.1 meters in terms of storm duration

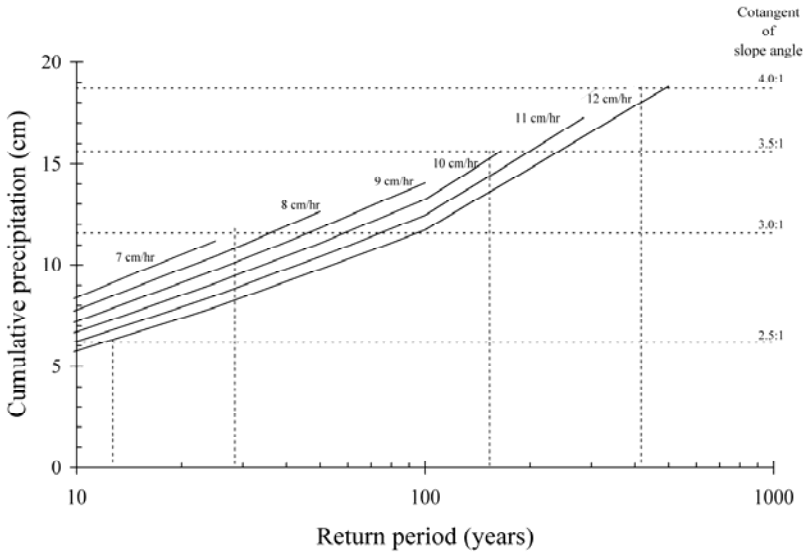

Figure 9.5: Recurrence rate of failures for cracked Eagle Ford clay under Austin weather conditions given a failure depth of 1.1 meters in terms of storm duration considering events of less than 100 minute duration

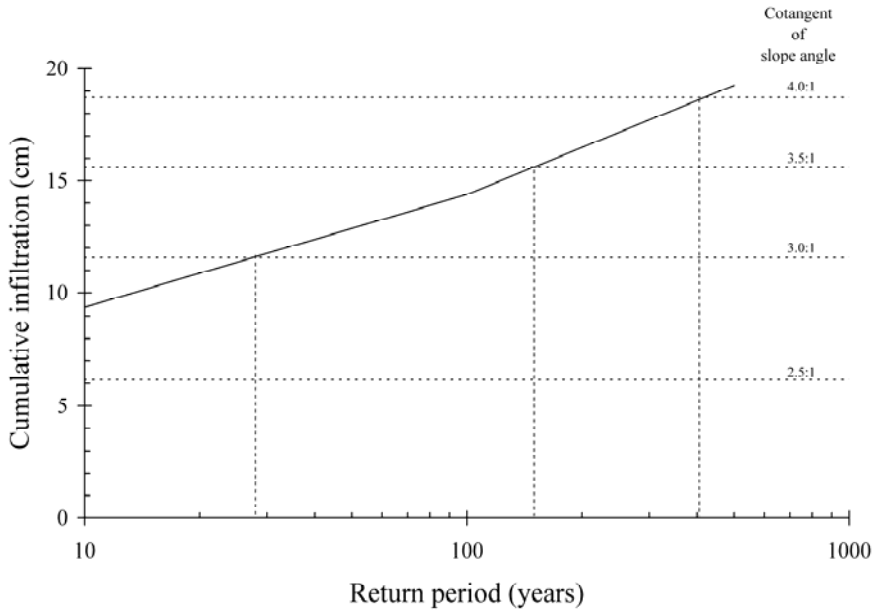

Figure 9.6: Recurrence rate of failures for cracked Eagle Ford clay under Austin weather conditions given a failure depth of 1.1 meters for a storm duration of 100 minutes

Chapter 10. Final Remarks

10.1. Significance of the Experimental Results on the Stability of High PI Clay Slopes after Discrete Precipitation Events

The results of the experimental component on hydraulic properties indicate that cracking changes the shape of the SMRC and the K-function of high PI clays. These changes have the potential to affect slope performance because they lead to significant increases in rates of water infiltration and evaporation. They also lead to the development of contrasting hydraulic conductivities between the zone subjected to moisture fluctuations and the intact clay zone.

The beneficial aspects of negative pore water pressures in slope stability are generally not considered in design because negative pore water pressures can be lost due to water infiltration. While this has been a commonly accepted design approach, what is revealing in this experimental study is that cracking significantly changes the SMRC of high PI clay. As a result, comparatively high suction values may not develop unless the soil reaches significantly low volumetric water contents. This may be particularly detrimental to the stability of shallow slopes, where suction can lead to increased effective stress and increased shear strength.

The experimental results showed a significant increase in the hydraulic conductivity of unsaturated high PI clay due to cracking. Accordingly, the rate of infiltration into the slope will increase and may lead to destabilizing flow configurations. An increase in saturated hydraulic conductivity with cracking was also reported in past research (Boyton and Daniel 1980; Sims et al. 1996; and Albrecht and Benson 2001). If the depth of cracking is uniform, then there is also a potential for the development of distinct layers with significantly different SMRCs and hydraulic conductivities. Such multilayered configurations may conceivably lead to the generation of positive pore water pressures at the interface between the cracked and intact zones after discrete precipitation events.

10.2. Significance of the Experimental Results on the Long-Term Stability of High PI Clay Slopes

The long-term stability of high PI clay slopes has been speculated to depend on long-term changes in suction within clay slopes, which may be the product of long-term exposure of the slope to the environment (Aubeny and Lytton 2003). In this case, the average weather conditions, rather than discrete precipitation events, should be quantified. The boundary conditions for infiltration and evaporation in high PI clay slopes were investigated in this study. Specifically, boundary conditions typical for Texas, boundary conditions used for this testing program, and boundary conditions assumed by Aubeny and Lytton (2003) were evaluated. As previously discussed (see Figure 4.1), the effect of temperature on suction is minor when compared to the effect of relative humidity typical of Texas.

The range in atmospheric relative humidity values is very broad for the state of Texas. A map of annual mean relative humidity values throughout Texas at 6 a.m. and 6 p.m. is shown in Figure 10.1 (Arbingast et al. 1976). Based on these relative humidity values, a map showing the suction of surficial soil that reached equilibrium with atmospheric conditions in Texas is shown in Figure 10.2. Suction values were calculated using Equation 4.1 and assuming an average temperature of 20°C. The majority of surficial clays in Texas fall within the eastern half of Texas

(Olive et al. 1989). Suction values for surficial soils in the eastern half of Texas range from approximately 14,000 kPa to 107,000 kPa.

Results obtained in Section 4 indicate that evaporation occurs for relative humidity values below 97% (i.e., suctions greater than 3,800 kPa) in Eagle Ford Clay placed within 3 percent of optimum water content with standard Proctor compactive effort. These results indicate that a long-term evaporation process (and not a decrease in suction) is expected to take place for embankments constructed using typical soil placement conditions and for average relative humidity values in Texas.

Aubeny and Lytton (2003) assumed a scenario in which the long-term process involves continued decrease of suction (i.e., infiltration) from the surface into the slope. A diffusion coefficient was measured in the laboratory and used to model suction with time in the field. Flow was assumed to occur from the bottom of cracks into the slope. The suction at the bottom of the cracks was reported to range from 10 to 100 kPa and the suction under soil placement conditions was assumed to range between 300 and 1000 kPa. However, the results reported in this study indicate surface suctions ranging from 14,000 to 162,000 kPa (0) for average conditions in Texas and the suction under soil placement conditions ranging between 100 and 100,000 kPa. The long-term flow process involves continued desiccation (i.e., increase in suction) with time. Accordingly, the boundary conditions proposed by Aubeny and Lytton (2003) do not seem to be realistic.

10.3. Significance of the Experimental Results on the Selection of Shear Strength Values for Design

The measured fully softened secant friction angles of Eagle Ford Shale were compared to relationships for the fully softened secant friction angle by Stark et al. (2005) and Wright (2005). Both of these relationships appeared to show good agreement with the fully softened shear strength of the specimens subjected to wetting and drying. Considering that Wright (2005) also found good agreement between these relationships and the measured fully softened secant friction angles of Paris and Beaumont clay, it seems reasonable to conclude that these relationships may be used with confidence to select values of the fully softened secant friction angle for the design of high plasticity clay slopes. Specifically, the experimental results indicate that cyclic wetting and drying can cause a reduction in the strength of compacted high plasticity clays to the fully softened shear strength. The results from this study have confirmed that cyclic wetting and drying of compacted highly plastic clays and shales can reduce the shear strength to the fully softened state.

This study provides the suction profiles expected in high PI clays subjected to weather conditions typical of South and Central Texas. However, the results of two-dimensional and of infinite slope stability analysis indicate that positive pore water pressures are needed to induce failure in embankments with typical slopes. Based on the results of this investigation, it is recommended that the contribution of suction not be considered in the design of clay slopes. Instead, the effective shear strength of undisturbed clay should be used below the depth of moisture fluctuation, while the fully softened effective shear strength should be used within the zone of moisture fluctuations.

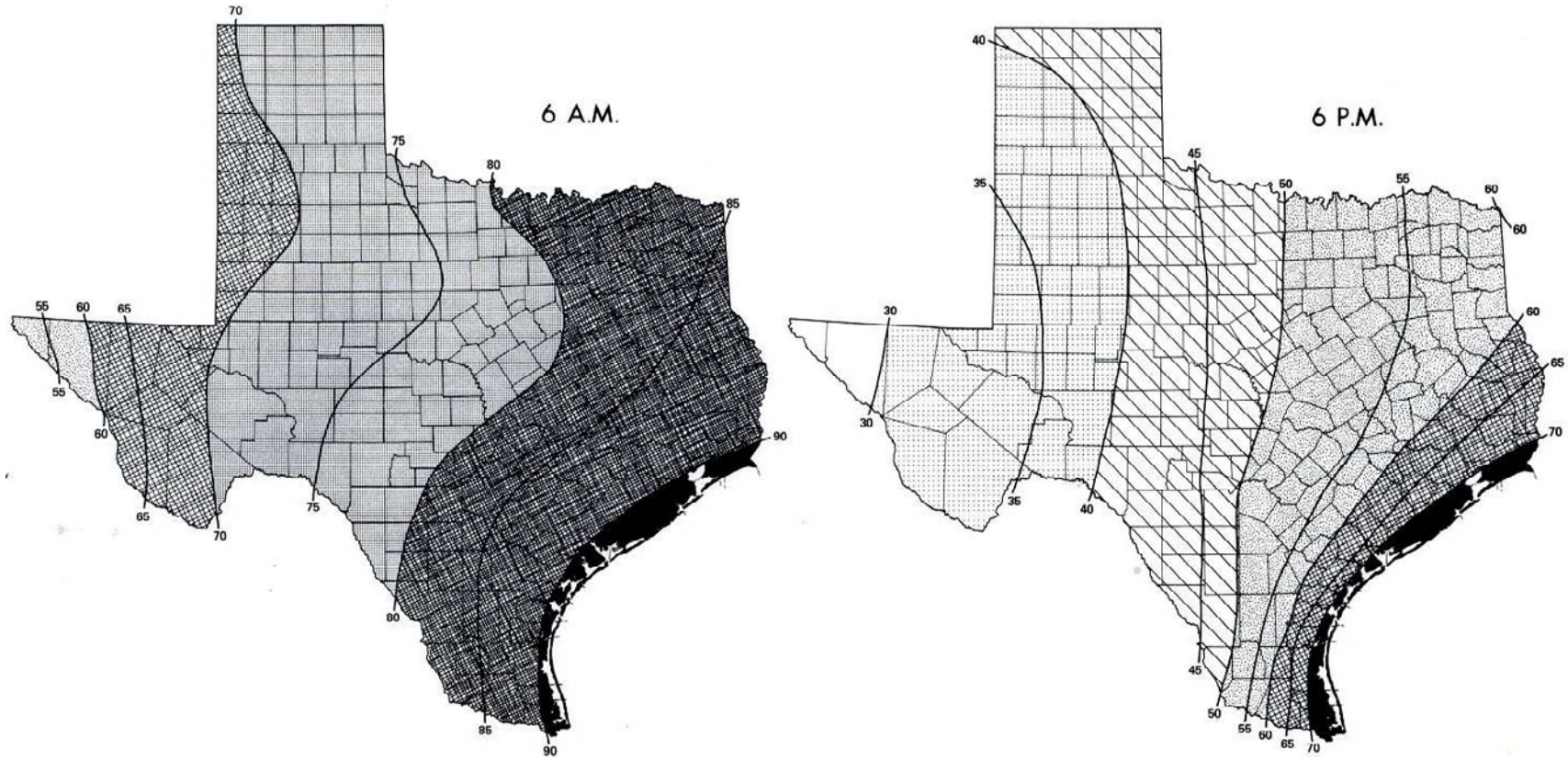

Figure 10.1: Mean annual relative humidity (Arbingast et al. 1976)

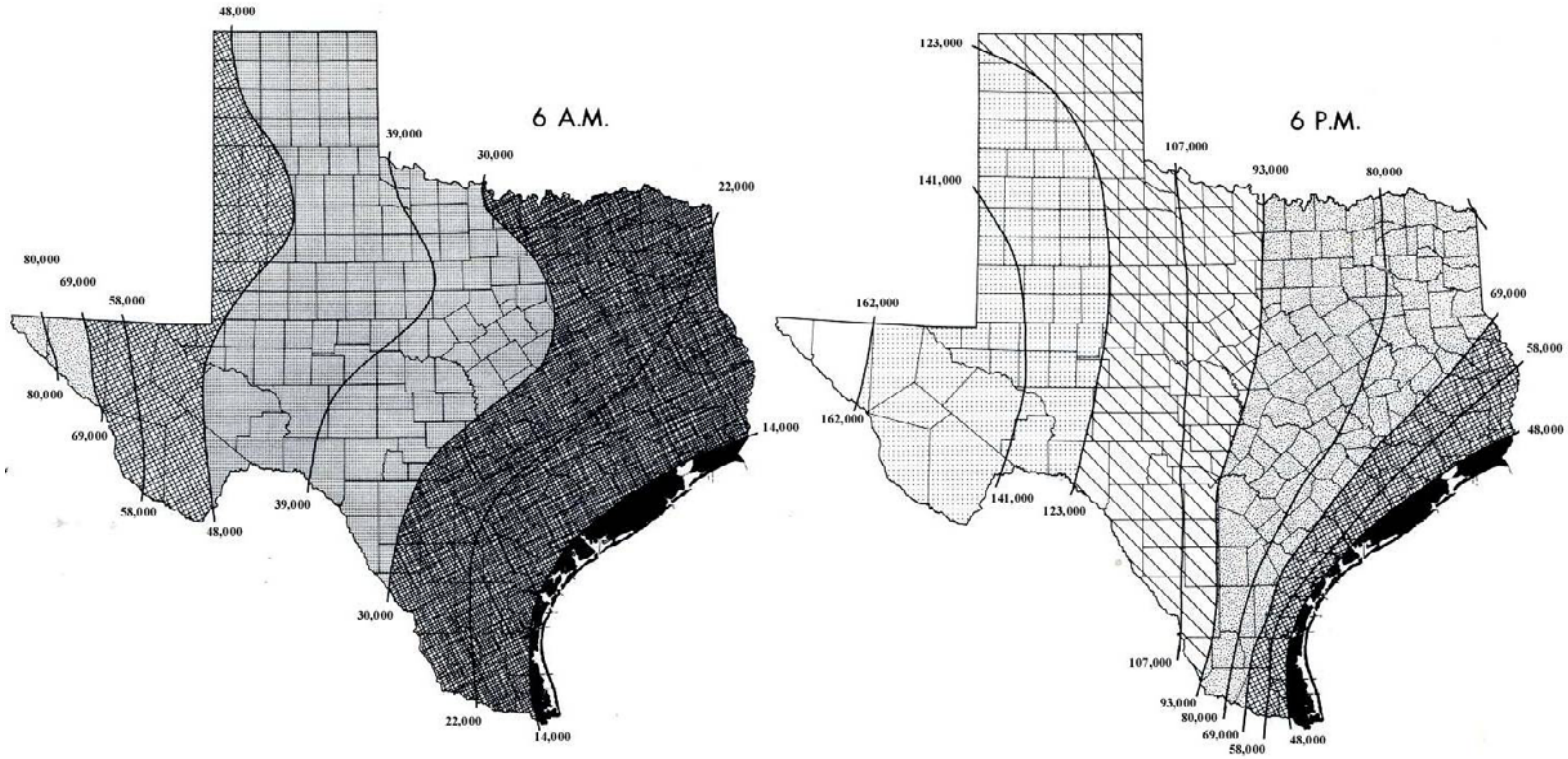

Figure 10.2: Equilibrium suction in kPa for 18.3°C calculated using Kelvin's equation (modified from Arbingast et al. 1976)

References

Albrecht, Brian A. and Benson, Craig H., 1996, "Effect of Desiccation on Compacted Natural Clays," *Journal of Geotechnical and Geoenvironmental Engineering*, Vol. 127, No. 1, pp. 67-76.

Arbingast, S., Kennamer, L, Ryan, R., Buchanan, J., Hezlep, W, Ellis, L., Jordan, T., Granger, C., and Zlatkovich, C. 1976. "Mean Annual Relative Humidity." *Atlas of Texas*, p. 19.

Aubeny, C., and Lytton, R., 2003, "Long-term Strength of Compacted High-PI clays," *Federal Highway Administration Report # TX-03/2100-1*, Project No. 0-2100.

Aubeny, C., and Lytton, R., 2004 "Shallow slides in compacted high plasticity clay slopes" *Journal of Geotechnical and Geoenvironmental Engineering*, Vol. 130, No. 7, July, pp. 717-727.

Bailey, B. and W. R. Stroman. 1992. "Slopes and Embankments in Eagle Ford Clays." In Proceedings of the Seventh International Conference on Expansive Soils, Volume 1 Held in Dallas, Texas August 3-5, 1992, 114-119.

Boynton, S, and Daniel, D, 1985, "Hydraulic conductivity tests on compacted clays." *Journal of Geotechnical and Geoenvironmental Engineering,* Vol. 111, No. 4, pp. 465-478.

Daniel, D., 1983, "Permeability test for unsaturated soil." *Geotechnical Testing Journal*, Vol. 6, No. 2, 81-86.

Duncan J. M., R. C. Horz, and T. L. Yang. 1989. "Shear Strength Correlations for Geotechnical Engineering." Virginia Polytechnic Institute and State University, Blacksburg, August, 1989, 100 pgs.

Galvan, Marcus, 10/2005, Personal Communication, Texas Department of Transportation Bridge Division, Austin, TX.

Gourlay, A.W. and Wright, S.G. 1984. "Initial Laboratory Study of the Shear Strength Properties of Compacted Highly Plastic Clays used for Highway Embankment Construction in the Area of Houston, Texas." *A Report on Laboratory Testing Performed under Inter-agency Contract No.'s (82-83)2187 and (84-85) 1026,* Center for Transportation Research, The University of Texas at Austin, (September 1984): 202 pgs.

Green, R. and S.G. Wright, "Factors Affecting the Long Term Strength of Compacted Beaumont Clay," Research Report 436-1, Center for Transportation Research, The University of Texas at Austin, October 1986.

Kayyal, M. K. and Wright S. G. 1991. "Investigation of Long-Term Strength Properties of Paris and Beaumont Clays in Earth Embankments," Research Report 1195-2F, Center for Transportation Research, The University of Texas at Austin, (November 1991):125 pgs.

Kelly, Hugh, 11/2007, Personal Communication, Parsons Brinckerhoff, Dallas, TX.

Kuhn, J., 2005, "Effect of Cracking on the Hydraulic Properties of Unsaturated Highly Plastic Clays." MS thesis, The University of Texas, Texas.

Lu, Ning, and Likos, William J, 2005, *Unsaturated Soil Mechanics*, Wiley, New York.

Meerdink, J., Benson, C., and Khire, M., 1996, "Unsaturated hydraulic conductivity of two compacted barrier soils." *Journal of Geotechnical Engineering*, Vol. 122, No. 7, pp. 565-576.

McKinney, Daene C. 2006. Course Notes for Hydrology, Austin, TX.

Wright, S. G. 2005. "Evaluation of Soil Shear Strengths for Slope and Retaining Wall Stability Analyses with Emphasis on High Plasticity Clays." *Project No. 5-1874-01*, Center for Transportation Research, The University of Texas at Austin, (August 2005): 90 pgs.

Sims, J., Elsworth, D., and Cherry, J., 1996, "Stress-dependent flow through fractured clay till: A laboratory study." *Canadian Geotechnical Journal*, Vol. 33, pp. 449-457.

Stark, T. D., H. Choi, and S. McCone. 2005. "Drained Shear Strength Parameters for Analysis of Landslides." *Journal of Geotechnical and Geoenvironmental Engineering* 131, no. 5 (May 1, 2005): 575-588.

Stauffer, P.A. and S.G. Wright, "An Examination of Earth Slope Failures in Texas," Research Report 353-3F, Center for Transportation Research, The University of Texas, November 1984.

Tindall, J.A., and Kunkel, J.R., 1999, *Unsaturated Zone Hydrology for Scientists and Engineers*, Prentice Hall, New Jersey.

Wendroth, O., Ehlers, W., Hopmans, J., Kage, H., Halbertsma, J., and Wösten, J.H., 1993 "Reevaluation of the Evaporation Method for Determining Hydraulic Functions in Unsaturated Soils." *Soil Science Society of America Journal*, Vol. 57, 1436-1443.